cell membrane and whether the GM1-like epitopes are unmasked. Colocalization and *cis*-interaction of gangliosides may either enable or inhibit antibody binding to the neuronal membrane or have no effect (Greenshields et al., 2009). In our recent study, the epitope targeted by monoclonal anti-GA1 antibody was masked in a glycolipid complex GA1/GQ1b, whereas that recognized by the monoclonal anti-GQ1b antibody was preserved (Ogawa et al., 2009). Therefore, even if GA1 and GQ1b actually form complexes in the biological membrane, the anti-GQ1b antibody can access GQ1b epitopes in GA1/GQ1b but the anti-GA1 antibody cannot access GA1 epitopes in the same complex. Thus, the local glycolipid environment in the plasma membrane may regulate the pathogenic effect of antiganglioside antibodies, and it should be borne in mind that the antibody–antigen interaction depends not only upon the fine specificity of individual antibodies but also upon the conformation of glycoepitopes formed in glycolipid environments in the nerve cell membrane.

7. Putative factors influencing antibody binding to target epitopes

Certain specific conditions of glycoepitopes in the cell membrane are essential for exertion of the pathogenic action of antiganglioside antibodies. First, complex glycolipid environments in the cell membrane may influence the accessibility and avidity of antiganglioside antibodies for target gangliosides, as described above (Fig. 3) (Kaida et al., 2008a; Greenshields et al., 2009). Analyses of the reactivity of antiganglioside antibodies against various GSCs are useful for evaluation of the accessibility of the antibodies. Second, the large amount of targeted gangliosides in particular loci of peripheral nerves is closely associated with antibody-mediated injury and specific clinical features. GQ1b is abundantly distributed in human oculomotor, trochlear, and abducens nerves, leading to predisposition to binding of anti-GQ1b antibodies (Chiba et al., 1993, 1997). Anti-GD1a antibody-mediated nerve injury is observed in GD3-synthase knockout mice that overexpress GD1a, but not in normal mice, probably because the abundant expression of GD1a at a particular region is critical for development of anti-GD1a-mediated nerve damage (Goodfellow et al., 2005). Third, the conformational difference of glycoepitopes between motor and sensory nerves may influence antibody binding and development of nerve injury. Ganglioside analysis of human motor and sensory nerves has shown that the amount of GM1 and GD1a is almost equal in both nerves, but that the ceramide compositions differ between the motor and sensory nerves (Ogawa-Goto et al., 1990): the gangliosides from sensory nerves are abundant in long-chain fatty acids, in contrast to those from motor nerves. In a binding assay using derivatives of GD1a bearing very long chain fatty acids, the difference in length of fatty acids in the ceramide reduced the binding ability of monoclonal anti-GD1a antibodies with GD1a derivatives, indicating that the ceramide composition can modify the steric structure of gangliosides in membranes (Tagawa et al., 2002). These findings may partly explain the preferential binding of anti-GD1a antibodies from AMAN patients to GD1a in motor nerves (Gong et al., 2002).

Finally, the conformational microstructure of sialic acids in gangliosides may regulate the binding ability of antiganglioside antibodies. In a recent immunohistochemical study using GD1a derivatives with chemically modified sialic acid residues, anti-GD1a monoclonal antibodies that preferentially stained motor axons specifically bound to GD1a-1-ethyl ester, GD1a-1-alcohol, and GD1a-1-methyl ester, in contrast to other anti-GD1a monoclonal antibodies that stained both motor and sensory axons (Lopez et al., 2008). There were no differences in binding to GD1a derivatives between anti-GD1a antibodies from AMAN patients and motor-specific anti-GD1a monoclonal antibodies. Thus, ganglioside exposure in the nerves and the fine specificity of antiganglioside antibodies is likely to regulate their accessibility to target gangliosides. The effects of phospholipids should also be considered because the presence of several kinds of phospholipids influences antibody binding to gangliosides (Hirakawa et al., 2005).

8. Perspective

Recent progress on the immunobiological mechanism in GBS has contributed to the precise understanding of antiganglioside antibody-mediated nerve dysfunction, and has encouraged development of novel therapeutic strategies for patients with GBS and its variants (Willison et al., 2008; Kaida and Kusunoki, 2009). Consideration of GSCs will provide new avenues of research on antibody–antigen interactions in GBS. Examination of anti-GSC antibodies may expand the spectrum of antiganglioside antibodies in GBS, enhancing their value as diagnostic markers and expediting understanding of the pathophysiology underlying antiganglioside antibody-mediated nerve dysfunction. New techniques such as combinatorial glycoarrays are beneficial for studies on anti-GSC antibodies (Rinaldi et al., 2009). The understanding of GSCs will also shed light on microdomain function mediated by carbohydrate–carbohydrate interactions in biological membranes. Microdomain function is controlled by carbohydrate-binding proteins such as selectins and Siglecs and is based on *cis*- or *trans*-carbohydrate–carbohydrate interactions (Hakomori, 2004; Varki, 2007). In the microdomain, complex glycoconjugates such as GSCs with clustered sialic acid epitopes may form rigid rodlike structures with multivalency and strict binding specificity, and are likely to function in cell–cell recognition or immune-mediated events in a more effective manner than a solo glycoepitope of an isolated ganglioside. This hypothesis is supported by a recent study demonstrating that a GSC, GM2/GM3, provides more efficient suppression of cell motility through blocking of cMet activation compared to GM2 or GM3 alone (Todeschini et al., 2008).

Acknowledgments

This work was supported by the Ministry of Education, Culture, Sports, Science and Technology of Japan (Grant-in-Aid for Scientific Research, 21390273) and the Ministry of Health, Labor, and Welfare of Japan (Research Grant for Neuroimmunological Diseases, H21-016, and Health Sciences Research Grant on Psychiatric and Neurological Diseases and Mental Health, H21-012).

References

Ang, C.W., Yuki, N., Jacobs, B.C., Koga, M., Van Doorn, P.A., Schmitz, P.I., Van Der Meche, F.G., 1999. Rapidly progressive, predominantly motor Guillain–Barré syndrome with anti-GalNAc-GD1a antibodies. Neurology 53, 2122–2127.

Arasaki, K., Kusunoki, S., Kudo, N., Kanazawa, I., 1993. Acute conduction block in vitro following exposure to antiganglioside sera. Muscle Nerve 16, 587–593.

Buchwald, B., Zhang, G., Vogt-Eisele, A.K., Zhang, W., Ahangari, R., Griffin, J.W., Hatt, H., Toyka, K.V., Sheikh, K.A., 2007. Anti-ganglioside antibodies alter presynaptic release and calcium influx. Neurobiol. Dis. 28, 113–121.

Chiba, A., Kusunoki, S., Shimizu, T., Kanazawa, I., 1992. Serum IgG antibody to ganglioside GQ1b is a possible marker of Miller Fisher syndrome. Ann. Neurol. 31, 677–679.

Chiba, A., Kusunoki, S., Obata, H., Machinami, R., Kanazawa, I., 1993. Serum anti-GQ1b IgG antibody is associated with ophthalmoplegia in Miller Fisher syndrome and Guillain–Barré syndrome: clinical and immunohistochemical studies. Neurology 43, 1911–1917.

Chiba, A., Kusunoki, S., Obata, H., Machinami, R., Kanazawa, I., 1997. Ganglioside composition of the human cranial nerves, with special reference to pathophysiology of Miller Fisher syndrome. Brain Res. 745, 32–36.

Corbo, M., Quattrini, A., Latov, N., Hays, A.P., 1993. Localization of GM1 and Gal(beta 1–3) GalNAc antigenic determinants in peripheral nerve. Neurology 43, 809–814.

Dilley, A., Gregson, N.A., Hadden, R.D., Smith, K.J., 2003. Effects on axonal conduction of anti-ganglioside sera and sera from patients with Guillain–Barre syndrome. J. Neuroimmunol. 139, 133–140.

Gong, Y., Tagawa, Y., Lunn, M.P., Laroy, W., Heffer-Lauc, M., Li, C.Y., Griffin, J.W., Schnaar, R.L., Sheikh, K.A., 2002. Localization of major gangliosides in the PNS: implications for immune neuropathies. Brain 125, 2491–2506.

Goodfellow, J.A., Bowes, T., Sheikh, K., Odaka, M., Halstead, S.K., Humphreys, P.D., Wagner, E.R., Yuki, N., Furukawa, K., Furukawa, K., Plomp, J.J., Willison, H.J., 2005. Overexpression of GD1a ganglioside sensitizes motor nerve terminals to anti-GD1a

antibody-mediated injury in a model of acute motor axonal neuropathy. J. Neurosci. 25, 1620–1628.
Goodyear, C.S., O'Hanlon, G.M., Plomp, J.J., Wagner, E.R., Morrison, I., Veitch, J., Cochrane, L., Bullens, R.W., Molenaar, P.C., Conner, J., Willison, H.J., 1999. Monoclonal antibodies raised against Guillain–Barré syndrome-associated *Campylobacter jejuni* lipopolysaccharides react with neuronal gangliosides and paralyze muscle–nerve preparations. J. Clin. Invest. 104, 697–708.
Greenshields, K.N., Halstead, S.K., Zitman, F.M., Rinaldi, S., Brennan, K.M., O'Leary, C., Chamberlain, L.H., Easton, A., Roxburgh, J., Pediani, J., Furukawa, K., Furukawa, K., Goodyear, C.S., Plomp, J.J., Willison, H.J., 2009. The neuropathic potential of anti-GM1 autoantibodies is regulated by the local glycolipid environment in mice. J. Clin. Invest. 119, 595–610.
Hafer-Macko, C.E., Sheikh, K.A., Li, C.Y., Ho, T.W., Cornblath, D.R., McKhann, G.M., Asbury, A.K., Griffin, J.W., 1996a. Immune attack on the Schwann cell surface in acute inflammatory demyelinating polyneuropathy. Ann. Neurol. 39, 625–635.
Hafer-Macko, C., Hsieh, S.T., Li, C.Y., Ho, T.W., Sheikh, K., Cornblath, D.R., McKhann, G.M., Asbury, A.K., Griffin, J.W., 1996b. Acute motor axonal neuropathy: an antibody-mediated attack on axolemma. Ann. Neurol. 40, 635–644.
Hakomori, S., 2000. Cell adhesion/recognition and signal transduction through glycosphingolipid microdomain. Glycoconj. J. 17, 143–151.
Hakomori, S., 2004. Carbohydrate-to-carbohydrate interaction, through glycosynapse, as a basis of cell recognition and membrane organization. Glycoconj. J. 21, 125–137.
Halstead, S.K., O'Hanlon, G.M., Humphreys, P.D., Morrison, D.B., Morgan, B.P., Todd, A.J., Plomp, J.J., Willison, H.J., 2004. Anti-disialoside antibodies kill perisynaptic Schwann cells and damage motor nerve terminals via membrane attack complex in a murine model of neuropathy. Brain 127, 2109–2123.
Halstead, S.K., Humphreys, P.D., Goodfellow, J.A., Wagner, E.R., Smith, R.A., Willison, H.J., 2005. Complement inhibition abrogates nerve terminal injury in Miller Fisher syndrome. Ann. Neurol. 58, 203–210.
Hao, Q., Saida, T., Yoshino, H., Kuroki, S., Nukina, M., Saida, K., 1999. Anti-GalNAc-GD1a antibody-associated Guillain–Barré syndrome with a predominantly distal weakness without cranial nerve impairment and sensory disturbance. Ann. Neurol. 45, 758–768.
Hirakawa, M., Morita, D., Tsuji, S., Kusunoki, S., 2005. Effects of phospholipids on anti-ganglioside antibody reactivity in GBS. J. Neuroimmunol. 159, 129–132.
Hirota, N., Kaji, R., Bostock, H., Shindo, K., Kawasaki, T., Mizutani, K., Oka, N., Kohara, N., Saida, T., Kimura, J., 1997. The physiological effect of anti-GM1 antibodies on saltatory conduction and transmembrane currents in single motor axons. Brain 120, 2159–2169.
Ho, T.W., Willison, H.J., Nachamkin, I., Li, C.Y., Veitch, J., Ung, H., Wang, G.R., Liu, R.C., Cornblath, D.R., Asbury, A.K., Griffin, J.W., McKhann, G.M., 1999. Anti-GD1a antibody is associated with axonal but not demyelinating forms of Guillain–Barré syndrome. Ann. Neurol. 45, 168–173.
Ilyas, A.A., Li, S.C., Chou, D.K., Li, Y.T., Jungalwala, F.B., Dalakas, M.C., Quarles, R.H., 1988. Gangliosides GM2, IV4GalNAcGM1b, and IV4GalNAcGC1a as antigens for monoclonal immunoglobulin M in neuropathy associated with gammopathy. J. Biol. Chem. 263, 4369–4373.
Jacobs, B.C., van Doorn, P.A., Schmitz, P.I., Tio-Gillen, A.P., Herbrink, P., Visser, L.H., Hooijkass, H., van der Meche, F.G., 1996. *Campylobacter jejuni* infections and anti-GM1 antibodies in Guillain–Barré syndrome. Ann. Neurol. 40, 181–187.
Kaida, K., Kusunoki, S., Kamakura, K., Motoyoshi, K., Kanazawa, I., 2001. Guillain-Barré syndrome with IgM antibody to the ganglioside GalNAc-GD1a. J. Neuroimmunol. 113, 260–267.
Kaida, K., Kusunoki, S., 2009. Guillain–Barré syndrome — update on immunobiology and treatment. Expert Rev. Neurother. 9, 1307–1319.
Kaida, K., Kusunoki, S., Kamakura, K., Motoyoshi, K., Kanazawa, I., 2000. Guillain–Barre syndrome with antibody to a ganglioside, N-acetylgalactosaminyl GD1a. Brain 123, 116–124.
Kaida, K., Kusunoki, S., Kamakura, K., Motoyoshi, K., Kanazawa, I., 2003. GalNAc-GD1a in human peripheral nerve. Target sites of anti-ganglioside antibody. Neurology 61, 465–470.
Kaida, K., Morita, D., Kanzaki, M., Kamakura, K., Motoyoshi, K., Hirakawa, M., Kusunoki, S., 2004. Ganglioside complexes: as new target antigens in Guillain–Barré syndrome. Ann. Neurol. 56, 567–571.
Kaida, K., Kanzaki, M., Morita, D., Kamakura, K., Motoyoshi, K., Hirakawa, M., Kusunoki, S., 2006. Anti-ganglioside complex antibodies in Miller Fisher syndrome. J. Neurol. Neurosurg. Psychiatry 77, 1043–1046.
Kaida, K., Morita, D., Kanzaki, M., Kamakura, K., Motoyoshi, K., Hirakawa, M., Kusunoki, S., 2007. Anti-ganglioside complex antibodies associated with severe disability in GBS. J. Neuroimmunol. 182, 212–218.
Kaida, K., Kamakura, K., Ogawa, G., Ueda, M., Motoyoshi, K., Arita, M., Kusunoki, S., 2008a. GD1b-specific antibody induces ataxia in Guillain–Barré syndrome. Neurology 71, 196–201.
Kaida, K., Sonoo, M., Ogawa, G., Kamakura, K., Ueda-Sada, M., Arita, M., Motoyoshi, K., Kusunoki, S., 2008b. GM1/GalNAc-GD1a complex: a target for pure motor Guillain–Barré syndrome. Neurology 71, 1683–1690.
Kaida, K., Ariga, T., Yu, R.K., 2009. Antiganglioside antibodies and their pathophysiological effects on Guillain–Barré syndrome and related disorders—a review. Glycobiology 19, 676–692.
Kanzaki, M., Kaida, K.-I., Ueda, M., Morita, D., Hirakawa, M., Motoyoshi, K., Kamakura, K., Kusunoki, S., 2008. Ganglioside complexes containing GQ1b as targets in Miller Fisher and Guillain–Barré syndromes. J. Neurol. Neurosurg. Psychiatry 79, 1148–1152.
Koga, M., Tatsumoto, M., Yuki, N., Hirata, K., 2001. Range of cross reactivity of anti-GM1 IgG antibody in Guillain–Barré syndrome. J. Neurol. Neurosurg. Psychiatry 71, 123–124.
Koga, M., Yoshino, H., Morimatsu, M., Yuki, N., 2002. Anti-GT1a IgG in Guillain–Barré syndrome. J. Neurol. Neurosurg. Psychiatry 72, 767–771.
Kuijf, M.L., Godschalk, P.C., Gilbert, M., Endtz, H.P., Tio-Gillen, A.P., van Ang, C.W., Doorn, P.A., Jacobs, B.C., 2007. Origin of ganglioside complex antibodies in Guillain–Barré syndrome. J. Neuroimmunol. 188, 69–73.
Kusunoki, S., Chiba, A., Tai, T., Kanazawa, I., 1993. Localization of GM1 and GD1b antigens in the human peripheral nervous system. Muscle Nerve 16, 752–756.
Kusunoki, S., Iwamori, M., Chiba, A., Hitoshi, S., Arita, M., Kanazawa, I., 1996a. GM1b is a new member of antigen for serum antibody in Guillain–Barré syndrome. Neurology 47, 237–242.
Kusunoki, S., Shimizu, J., Chiba, A., Ugawa, Y., Hitoshi, S., Kanazawa, I., 1996b. Experimental sensory neuropathy induced by sensitization with ganglioside GD1b. Ann. Neurol. 39, 424–431.
Kusunoki, S., Hitoshi, S., Kaida, K., Arita, M., Kanazawa, I., 1999a. Monospecific anti-GD1b IgG is required to induce rabbit ataxic neuropathy. Ann. Neurol. 45, 400–403.
Kusunoki, S., Chiba, A., Kanazawa, I., 1999b. Anti-GQ1b IgG antibody is associated with ataxia as well as ophthalmoplegia. Muscle Nerve 22, 1071–1074.
Kuwabara, S., Yuki, N., Koga, M., Hattori, T., Matsuura, D., Miyake, M., Noda, M., 1998. IgG anti-GM1 antibody is associated with reversible conduction failure and axonal degeneration in Guillain–Barré syndrome. Ann. Neurol. 44, 202–208.
Kuwabara, S., Ogawara, K., Sung, J.Y., Mori, M., Kanai, K., Hattori, T., Yuki, N., Lin, C.S., Burke, D., Bostock, H., 2002. Differences in membrane properties of axonal and demyelinating Guillain–Barre syndromes. Ann. Neurol. 52, 180–187.
Lehmann, H.C., Lopez, P.H., Zhang, G., Ngyuen, T., Zhang, J., Kieseier, B.C., Mori, S., Sheikh, K.A., 2007. Passive immunization with anti-ganglioside antibodies directly inhibits axon regeneration in an animal model. J. Neurosci. 27, 27–34.
Liu, J.X., Willison, H.J., Pedrosa-Domellöf, F., 2009. Immunolocalization of GQ1b and related gangliosides in human extraocular neuromuscular junctions and muscle spindles. Invest. Ophthalmol. Vis. Sci. 50, 3226–3232.
Lopez, P.H.H., Schnaar, R.L., 2009. Gangliosides in cell recognition and membrane protein regulation. Curr. Opin. Struct. Biol. 19, 1–9.
Lopez, P.H., Zhang, G., Bianchet, M.A., Schnaar, R.L., Sheikh, K.A., 2008. Structural requirements of anti-GD1a antibodies determine their target specificity. Brain 131, 1926–1939.
Lu, J.L., Sheikh, K.A., Wu, H.S., Zhang, J., Jiang, Z.F., Cornblath, D.R., McKhann, G.M., Asbury, A.K., Griffin, J.W., Ho, T.W., 2000. Physiologic–pathologic correlation in Guillain–Barré syndrome in children. Neurology 54, 33–39.
Martin, P.T., 2003. Glycobiology of the neuromuscular junction. J. Neurocytol. 32, 915–929.
Miyazaki, T., Kusunoki, S., Kaida, K., Shiina, M., Kanazawa, I., 2001. Guillain–Barré syndrome associated with IgG monospecific to ganglioside GD1b. Neurology 56, 1227–1229.
Nagashima, T., Koga, M., Odaka, M., Hirata, K., Yuki, N., 2004. Clinical correlates of serum anti-GT1a IgG antibodies. J. Neurol. Sci. 219, 139–145.
Nagashima, T., Koga, M., Odaka, M., Hirata, K., Yuki, N., 2007. Continuous spectrum of pharyngeal–cervical–brachial variant of Guillain–Barré syndrome. Arch. Neurol. 64, 1519–1523.
Nakatani, Y., Nagaoka, T., Hotta, S., Utsunomiya, I., Yoshino, H., Miyatake, T., Hoshi, K., Taguchi, K., 2007. IgG anti-GalNAc-GD1a antibody inhibits the voltage-dependent calcium channel currents in PC12 pheochromocytoma cells. Exp. Neurol. 204, 380–386.
Nakatani, Y., Hotta, S., Utsunomiya, I., Tanaka, K., Hoshi, K., Ariga, T., Yu, R.K., Miyatake, T., Taguchi, K., 2009. Cav2.1 voltage-dependent Ca^{2+} channel current is inhibited by serum from select patients with Guillain–Barré syndrome. Neurochem. Res. 34, 149–157.
Odaka, M., Yuki, N., Hirata, K., 2001. Anti-GQ1b IgG antibody syndrome: clinical and immunological range. J. Neurol. Neurosurg. Psychiatry 70, 50–55.
Ogawa, G., Kaida, K., Kusunoki, S., Ueda, M., Kimura, F., Kamakura, K., 2009. Antibodies to ganglioside complexes consisting of asialo-GM1 and GQ1b or GT1a in Fisher and Guillain–Barré syndromes. J. Neuroimmunol. 214, 125–127.
Ogawa-Goto, K., Funamoto, N., Abe, T., Nagashima, K., 1990. Different ceramide compositions of gangliosides between human motor and sensory nerves. J. Neurochem. 55, 1486–1493.
Plomp, J.J., Molenaar, P.C., O'Hanlon, G.M., Jacobs, B.C., Veitch, J., Daha, M.R., van Doorn, P.A., van der Meche, F.G., Vincent, A., Morgan, B.P., Willison, H.J., 1999. Miller Fisher anti-GQ1b antibodies: alpha-latrotoxin-like effects on motor end plates. Ann. Neurol. 45, 189–199.
Putzu, G.A., Figarella-Branger, D., Bouvier-Labit, C., Liprandi, A., Bianco, N., Pellissier, J.F., 2000. Immunohistochemical localization of cytokines, C5b-9 and ICAM-1 in peripheral nerve of Guillain–Barré syndrome. J. Neurol. Sci. 174, 16–21.
Rees, J.H., Gregson, N.A., Hughes, R.A., 1995. Anti-ganglioside GM1 antibodies in Guillain–Barré syndrome and their relationship to *Campylobacter jejuni* infection. Ann. Neurol. 38, 809–816.
Rinaldi, S., Brennan, K.M., Goodyear, C.S., O'Leary, C., Schiavo, G., Crocker, P.R., Willison, H.J., 2009. Analysis of lectin binding to glycolipid complexes using combinatorial glycoarrays. Glycobiology 19, 789–796.
Santoro, M., Uncini, A., Corbo, M., Staugaitis, S.M., Thomas, F.P., Hays, A.P., Latov, N., 1992. Experimental conduction block induced by serum from a patient with anti-GM1 antibodies. Ann. Neurol. 31, 385–390.
Sheikh, K.A., Deerinck, T.J., Ellisman, M.H., Griffin, J.W., 1999. The distribution of ganglioside-like moieties in peripheral nerves. Brain 122, 449–460.
Simons, K., Toomre, D., 2000. Lipid rafts and signal transduction. Nat. Rev. Mol. Cell Biol. 1, 31–39.
Susuki, K., Nishimoto, Y., Yamada, M., Baba, M., Ueda, S., Hirata, K., Yuki, N., 2003. Acute motor axonal neuropathy rabbit model: immune attack on nerve root axons. Ann. Neurol. 54, 383–388.
Susuki, K., Baba, H., Tohyama, K., Kanai, K., Kuwabara, S., Hirata, K., Furukawa, K., Furukawa, K., Rasband, M.N., Yuki, N., 2007a. Gangliosides contribute to stability of

paranodal junctions and ion channel clusters in myelinated nerve fibers. Glia 55, 746–757.
Susuki, K., Rasband, M.N., Tohyama, K., Koibuchi, K., Okamoto, S., Funakoshi, K., Hirata, K., Baba, H., Yuki, N., 2007b. Anti-GM1 antibodies cause complement-mediated disruption of sodium channel clusters in peripheral motor nerve fibers. J. Neurosci. 27, 3956–3967.
Svennerholm, L., Månsson, J.E., Li, Y.T., 1973. Isolation and structural determination of a novel ganglioside, a disialosylpentahexosylceramide from human brain. J. Biol. Chem. 248, 740–742.
Tagawa, Y., Laroy, W., Nimrichter, L., Fromholt, S.E., Moser, A.B., Moser, H.W., Schnaar, R.L., 2002. Anti-ganglioside antibodies bind with enhanced affinity to gangliosides containing very long chain fatty acids. Neurochem. Res. 27, 847–855.
Taguchi, K., Ren, J., Utsunomiya, I., Aoyagi, H., Fujita, N., Ariga, T., Miyatake, T., Yoshino, H., 2004. Neurophysiological and immunohistochemical studies on Guillain–Barré syndrome with IgG anti-GalNAc-GD1a antibodies—effects on neuromuscular transmission. J. Neurol. Sci. 225, 91–98.
Takada, K., Shimizu, J., Kusunoki, S., 2008. Apoptosis of primary sensory neurons in GD1b-induced sensory ataxic neuropathy. Exp. Neurol. 209, 279–283.
Takigawa, T., Yasuda, H., Kikkawa, R., Shigeta, Y., Saida, T., Kitasato, H., 1995. Antibodies against GM1 ganglioside affect K + and Na + currents in isolated rat myelinated nerve fibers. Ann. Neurol. 37, 436–442.
Todeschini, A.R., Dos Santos, J.N., Handa, K., Hakomori, S.-I., 2008. Ganglioside GM2/GM3 complex affixed on silica nanospheres strongly inhibits cell motility through CD82/cMet-mediated pathway. Proc. Natl. Acad. Sci. U. S. A. 105, 1925–1930.
Varki, A., 2007. Glycan-based interactions involving vertebrate sialic-acid-recognizing proteins. Nature 446, 1023–1029.
Visser, L.H., Van der Meche, F.G., Van Doorn, P.A., Meulstee, J., Jacobs, B.C., Oomes, P.G., Kleyweg, R.P., Meulstee, J., 1995. Guillain–Barré syndrome without sensory loss (acute motor neuropathy). A subgroup with specific clinical, electrodiagnostic and laboratory features. Dutch Guillain–Barré Study Group. Brain 118, 841–847.
Wanschitz, J., Maier, H., Lassmann, H., Budka, H., Berger, T., 2003. Distinct time pattern of complement activation and cytotoxic T cell response in Guillain–Barré syndrome. Brain 126, 2034–2042.
Weber, F., Rudel, R., Aulkemeyer, P., Brinkmeier, H., 2000. Anti-GM1 antibodies can block neuronal voltage-gated sodium channels. Muscle Nerve 23, 1414–1420.
Willison, H.J., Yuki, N., 2002. Peripheral neuropathies and anti-glycolipid antibodies. Brain 125, 2591–2625.
Willison, H.J., Halstead, S.K., Beveridge, E., Zitman, F.M., Greenshields, K.N., Morgan, B.P., Plomp, J.J., 2008. The role of complement and complement regulators in mediating motor nerve terminal injury in murine models of Guillain–Barre syndrome. J. Neuroimmunol. 201–202, 172–182.
Yuki, N., Ang, C.W., Koga, M., Jacobs, B.C., van Doorn, P.A., Hirata, K., van der Meche, F.G., 2000. Clinical features and response to treatment in Guillain–Barré syndrome associated with antibodies to GM1b ganglioside. Ann. Neurol. 47, 314–321.
Yuki, N., Yamada, M., Koga, M., Odaka, M., Susuki, K., Tagawa, Y., Ueda, S., Kasama, T., Ohnishi, A., Hayashi, S., Takahashi, H., Kamijo, M., Hirata, K., 2001. Animal model of axonal Guillain–Barré syndrome induced by sensitization with GM1 ganglioside. Ann. Neurol. 49, 712–720.
Yuki, N., Susuki, K., Koga, M., Nishimoto, Y., Odaka, M., Hirata, K., Taguchi, K., Miyatake, T., Furukawa, K., Kobata, T., Yamada, M., 2004. Carbohydrate mimicry between human ganglioside GM1 and *Campylobacter jejuni* lipooligosaccharide causes Guillain–Barré syndrome. Proc. Natl. Acad. Sci. U. S. A. 101, 11404–11409.

Cellular/Molecular

N-Acetylglucosamine 6-*O*-Sulfotransferase-1-Deficient Mice Show Better Functional Recovery after Spinal Cord Injury

Zenya Ito,[1,2] Kazuma Sakamoto,[1]* Shiro Imagama,[1,2]* Yukihiro Matsuyama,[2] Haoqian Zhang,[1] Kenichi Hirano,[2] Kei Ando,[2] Toshihide Yamashita,[3] Naoki Ishiguro,[2] and Kenji Kadomatsu[1,4]

Departments of [1]Biochemistry and [2]Orthopedics, Nagoya University Graduate School of Medicine, Nagoya 466-8550, Japan, [3]Department of Molecular Neuroscience, Graduate School of Medicine, Osaka University, Osaka 565-0871, Japan, and [4]Institute for Advanced Research, Nagoya University, Nagoya 464-8601, Japan

Neurons in the adult CNS do not spontaneously regenerate after injuries. The glycosaminoglycan keratan sulfate is induced after spinal cord injury, but its biological significance is not well understood. Here we investigated the role of keratan sulfate in functional recovery after spinal cord injury, using mice deficient in *N*-acetylglucosamine 6-*O*-sulfotransferase-1 that lack 5D4-reactive keratan sulfate in the CNS. We made contusion injuries at the 10th thoracic level. Expressions of *N*-acetylglucosamine 6-*O*-sulfotransferase-1 and keratan sulfate were induced after injury in wild-type mice, but not in the deficient mice. The wild-type and deficient mice showed similar degrees of chondroitin sulfate induction and of CD11b-positive inflammatory cell recruitment. However, motor function recovery, as assessed by the footfall test, footprint test, and Basso mouse scale locomotor scoring, was significantly better in the deficient mice. Moreover, the deficient mice showed a restoration of neuromuscular system function below the lesion after electrical stimulation at the occipito-cervical area. In addition, axonal regrowth of both the corticospinal and raphespinal tracts was promoted in the deficient mice. *In vitro* assays using primary cerebellar granule neurons demonstrated that keratan sulfate proteoglycans were required for the proteoglycan-mediated inhibition of neurite outgrowth. These data collectively indicate that keratan sulfate expression is closely associated with functional disturbance after spinal cord injury. *N*-acetylglucosamine 6-*O*-sulfotransferase-1-deficient mice are a good model to investigate the roles of keratan sulfate in the CNS.

Introduction

Neurons in the adult mammalian CNS do not spontaneously regenerate after injuries. Many factors contribute to this lack of repair, including a lack of growth-promoting factors (Widenfalk et al., 2001), the poor intrinsic regenerative capacity of CNS neurons (Neumann and Woolf, 1999), inhibitory factors associated with CNS myelin (Filbin, 2003; McGee and Strittmatter, 2003; Schwab, 2004), chemorepulsive molecules (De Winter et al., 2002), and glial scar-associated inhibitors such as chondroitin sulfate (CS) proteoglycans (CSPGs) (Silver and Miller, 2004).

The extracellular matrix of the adult CNS has a unique composition. Instead of collagens, laminin-1, and fibronectin, this matrix is rich in hyaluronic acid and CSPGs (Ruoslahti, 1996). CSPGs are reinduced after injury and inhibit neuronal axon regrowth. The inhibitory function of CSPGs on axonal outgrowth is primarily ascribed to their covalently attached CS-glycosaminoglycans, since the ablation of CS by use of chondroitinase ABC or a DNA enzyme that acts on xylosyltransferase enhances neuronal axon growth in CNS injury (Moon et al., 2001; Bradbury et al., 2002; Grimpe and Silver, 2004). For example, the axon growth of dopamine neurons is enhanced by chondroitinase ABC treatment after nigrostriatal tract transaction (Moon et al., 2001). Chondroitinase ABC treatment has been shown to enhance functional recovery after spinal cord injury in a rat model (Bradbury et al., 2002). It is known that CSPGs activate the Rho–Rho kinase pathway via an unknown receptor, leading to suppression of axonal growth (Borisoff et al., 2003; Mueller et al., 2005).

Keratan sulfate (KS) is another glycosaminoglycan. It is composed of repeating disaccharide units of galactose and *N*-acetylglucosamine (GlcNAc), where the C6 position of GlcNAc is always sulfated. The 5D4 antibody is commonly used for detection of KS, and it has been demonstrated that 5D4-reactive KS is induced in a rat model of spinal cord injury (Jones and Tuszynski, 2002). The reaction sequence for the biosynthesis of KS consists of *N*-acetylglucosaminylation, 6-sulfation of a GlcNAc residue exposed at the nonreducing end, and galactosylation (Habuchi et al., 2006; Kitayama et al., 2007). Because GlcNAc sulfation at the C6 position is necessary for KS chain elongation (Kitayama et al., 2007), failure of this sulfation leads to loss of KS synthesis. That is, deficiency of human *N*-acetylglucosamine 6-*O*-sulfotransferase-5 (GlcNAc6ST-5) leads to loss of corneal KS synthesis (Akama et al., 2000), and lack of mouse GlcNAc6ST-1 causes loss of 5D4-reactive KS expression in the CNS (Zhang et

Received June 2, 2009; revised Dec. 15, 2009; accepted March 8, 2010.

This work was supported in part by Ministry of Education, Culture, Sports, Science and Technology (MEXT) Grants-in-Aid 18390099 and 20390092 to K.K.; by funds from the 21st Century Centers of Excellence (COE) Program and Global COE Program of MEXT to Nagoya University; and by the Uehara Foundation. We thank T. Muramatsu (Aichi Gakuin University, Nagoya, Japan) for continuous support of this study.

*K.S. and S.I. contributed equally to this work.

Correspondence should be addressed to Kenji Kadomatsu, Department of Biochemistry, Nagoya University Graduate School of Medicine, 65 Tsurumai-cho, Aichi 466-8550, Japan. E-mail: kkadoma@med.nagoya-u.ac.jp.

DOI:10.1523/JNEUROSCI.2570-09.2010

 0270-6474/10/305937-11$15.00/0

al., 2006). In this study, to investigate the biological significance of KS in neurological function, we applied a contusion spinal cord injury model to *N*-acetylglucosamine 6-*O*-sulfotransferase-1-deficient mice and found that these mice showed better functional recovery than their wild-type counterparts.

Materials and Methods

Mice. GlcNAc6ST-1−/− mice were produced using D3 embryonic stem cells and an ordinary gene-targeting technology as described previously (Hemmerich et al., 2001). GlcNAc6ST-1+/− mice obtained after backcrossing with C57BL/6J for more than 11 generations were interbred. The littermates obtained were used for the spinal cord injury experiments. These mice were maintained in the animal facilities of Nagoya University. All experiments were performed in accordance with protocols approved by the institutional animal committee.

Spinal cord injury model. We anesthetized adult C57BL/6J mice, their wild-type littermates, and GlcNAc6ST-1−/− mice (female, 8 weeks old, 20–30 g) using an intraperitoneal injection of pentobarbital sodium (50 mg/kg). After laminectomy at the 10th thoracic spinal lamina, we exposed the dorsal surface of the dura mater. A bilateral contusion injury was created by delivering a 100 kdyn force to the cord using a commercially available spinal cord injury device (Infinite Horizon Impactor; Precision Systems and Instrumentation). Sham controls were subjected to laminectomy only. As postoperative care, the bladder was compressed by manual abdominal pressure twice per day until bladder function was restored, and prophylactic antibiotic treatment [1.0 ml of Bactramin (Roche) in 500 ml of acidified water] was maintained for 1 week. The numbers of mice used and mortality are summarized in supplemental Table 1 (available at www.jneurosci.org as supplemental material).

Reagents. Anti-KS 5D4 and anti-CS CS-56 monoclonal antibodies were purchased from Seikagaku. A biotin labeling kit-NH2 was used for biotinylation of the 5D4 antibody and purchased from Dojindo Molecular Technologies. CD11b monoclonal antibody was from BioLegend; Cy3-conjugated anti-glial fibrillary acidic protein (GFAP) monoclonal antibody was from Sigma; anti-Iba1 polyclonal rabbit antibody was from Wako; anti-platelet-derived growth factor receptor (PDGFr) polyclonal rabbit antibody was from Thermo Fisher Scientific Anatomical Pathology; anti-GAP-43 polyclonal rabbit antibody was from Millipore Bioscience Research Reagents; anti-serotonin (5HT) polyclonal rabbit antibody was from ImmunoStar; anti-type IV collagen polyclonal rabbit antibody was from LSL; and protein kinase Cγ was from Santa Cruz Biotechnology. Cy3- or Cy2-conjugated streptavidin and Cy3-conjugated anti-mouse IgM were from Jackson ImmunoResearch; Cy3-conjugated anti-rabbit IgG was from Zymed; and fluorescein isothiocyanate (FITC)-conjugated anti-rat IgG was from Sigma. FluorSave was obtained from Calbiochem.

Immunohistochemistry. Mice were perfused transcardially under deep ether anesthesia with buffered 4% paraformaldehyde. The spinal cords were removed, postfixed in 4% paraformaldehyde overnight, and cryoprotected in buffered 30% sucrose during the subsequent night. Tissues were cut into 12 μm sections with a cryostat and mounted on glass slides. Sections were blocked in PBS containing 3% bovine serum albumin (BSA) and 5% normal mouse serum for staining of biotin-conjugated anti-KS 5D4 or blocked in PBS containing 1% BSA and 10% normal goat serum for other immunohistochemistry. Sections were then incubated with the primary antibodies at 100× dilution in a blocking solution overnight at 4°C in PBS containing 3% BSA and 5% normal mouse serum or overnight at 4°C in 1% BSA and 10% normal goat serum. After rinsing in PBS, the sections were incubated with the secondary antibody (Cy3- or Cy2-conjugated streptavidin, 1:100; Cy3-conjugated goat anti-rabbit IgG, 1:100; Cy3-conjugated goat anti-mouse IgM, 1:100; or FITC-conjugated goat anti-rat IgG, 1:100) for 60 min at room temperature. Subsequently, the sections were rinsed in PBS, mounted with FluorSave, and examined by confocal microscopy (MRC 1024; Bio-Rad). GAP-43 staining was performed using 3,30-diaminobenzidine (Wako).

Anterograde labeling of the cortico-spinal tract. Eight weeks after injury, descending corticospinal tract (CST) fibers were labeled with biotin-dextran amine (BDA; 10% in saline; 3.2 μl per cortex; molecular weight, 10,000; Invitrogen) injected under anesthesia at the left and the right motor cortices (coordinates: 2 mm posterior to the bregma, 2 mm lateral to the bregma, 0.5 mm depth). For each injection, 0.2 μl of BDA was delivered for a period of 30 s via a 15–20-μm-inner-diameter glass capillary attached to a microliter syringe (ITO). Two weeks after BDA injection, the animals were killed by perfusion with PBS followed by 4% paraformaldehyde. The spinal cords were dissected, postfixed overnight in the same fixatives, and cryopreserved in 30% sucrose in PBS. A 20 mm length of spinal cord 10 mm rostral and 10 mm caudal to the lesion site was embedded in Tissue Tek OCT. These blocks were sectioned in the transverse plane (25 μm). Sections were blocked in PBS with 0.3% Triton X-100 for 4 h and incubated for 2 h with Alexa Fluor 488-conjugated streptavidin (1:400; Invitrogen) in PBS with 0.05% Tween 20. We then took serial cross sections of the spinal cord and performed quantitative analysis of the distribution of the axons. Degrees of BDA uptake were assessed by counting the total number of fibers in the cross section 5 mm rostral to the lesioned site, where the CST was intact. For quantification of the number of labeled corticospinal axons 5 mm caudal to the lesion site, the number of labeled fibers was counted in the gray matter and divided by the number of labeled corticospinal axons 10 mm above the lesion for each animal. The labeled fibers were counted using MetaMorph software. Light intensity and thresholding values were maintained at constant levels for all analyses.

Reverse transcription-PCR. The forward primer 5′-AAGCCTACAGGTGGTGCGAA-3′ and reverse primer 5′-CAGGACTGTTAACCCGCTCA-3′ were used for reverse transcription (RT)-PCR for GlcNAc6ST-1 expression, and the forward primer 5′-GGTGGAGGTCGGAGTCAACG-3′ and reverse primer 5′-CAAAGTTGTCATGGATGACC-3′ were used for RT-PCR for glyceraldehyde 3-phosphate dehydrogenase (GAPDH) expression. SuperScript III reverse transcriptase (Invitrogen) was used to synthesize cDNA.

Morphometry. The epicenter of a lesion was determined by hematoxylin and eosin staining of several of the serial 12 μm sections. All the image analyses were performed using spinal cord samples prepared from six sagittal sections at 12 μm intervals (three sections on either side of the midline, which was identified by the appearance of the central tube), and all the axial image analyses in Figure 6 were performed using spinal cord samples from positions 5 mm caudal to the lesion site. Statistical analyses were performed for five mice for each experimental group. To count reactive astrocytes, standardized areas for sampling in six sections from each animal in each group were identified as a 600-μm-wide band of spinal cord adjoining the cord–lesion interface in each section.

Mean values for each animal were then compared. Light intensity and thresholding values were maintained at constant levels for all analyses by a computer-driven microscope stage (MetaMorph Offline version 6.3 r^2; Molecular Devices). The amounts of fibrous tissue and axonal outgrowth of the wound area were assessed by counting signals visualized by staining with anti-type IV collagen, CD11b, CS-56, GAP-43, and 5HT antibodies, respectively, for 640 × 2200 μm^2 counting frames around a lesion. Data were collected for at least five mice with each genotype in each experiment.

Footfall test. Mice were subjected to the grid runway test to assess locomotor function recovery at 6 weeks after injury. Performance on a wire grid was evaluated for 3 min by counting footfalls. A footfall was defined as either hindpaw missing a rung and extending through the space between adjacent grids. The wire grid was positioned flat and was 7 × 11 inches with grid squares of 0.35 × 0.35 inches. The number of footfalls was counted for five mice in each group.

Footprint test. In the footprint analysis, the hindpaws were covered with ink to record walking patterns during continuous locomotion across a paper runway (1.2 × 12 inches) at 6 weeks after injury, and the stride lengths were calculated. Strides were analyzed only when mice ran with constant velocity. All strides on the first and last 5 cm of the passage were excluded because of changing velocity.

Behavioral testing. The locomotor performance of animals was analyzed using the Basso mouse scale (BMS) open-field score (Basso et al., 2006) for 8 weeks, since the BMS has been shown to be a valid locomotor rating scale for mice. The evaluations were made by two blind observers for all analyzed groups. Briefly, the BMS is a nine-point scale that pro-

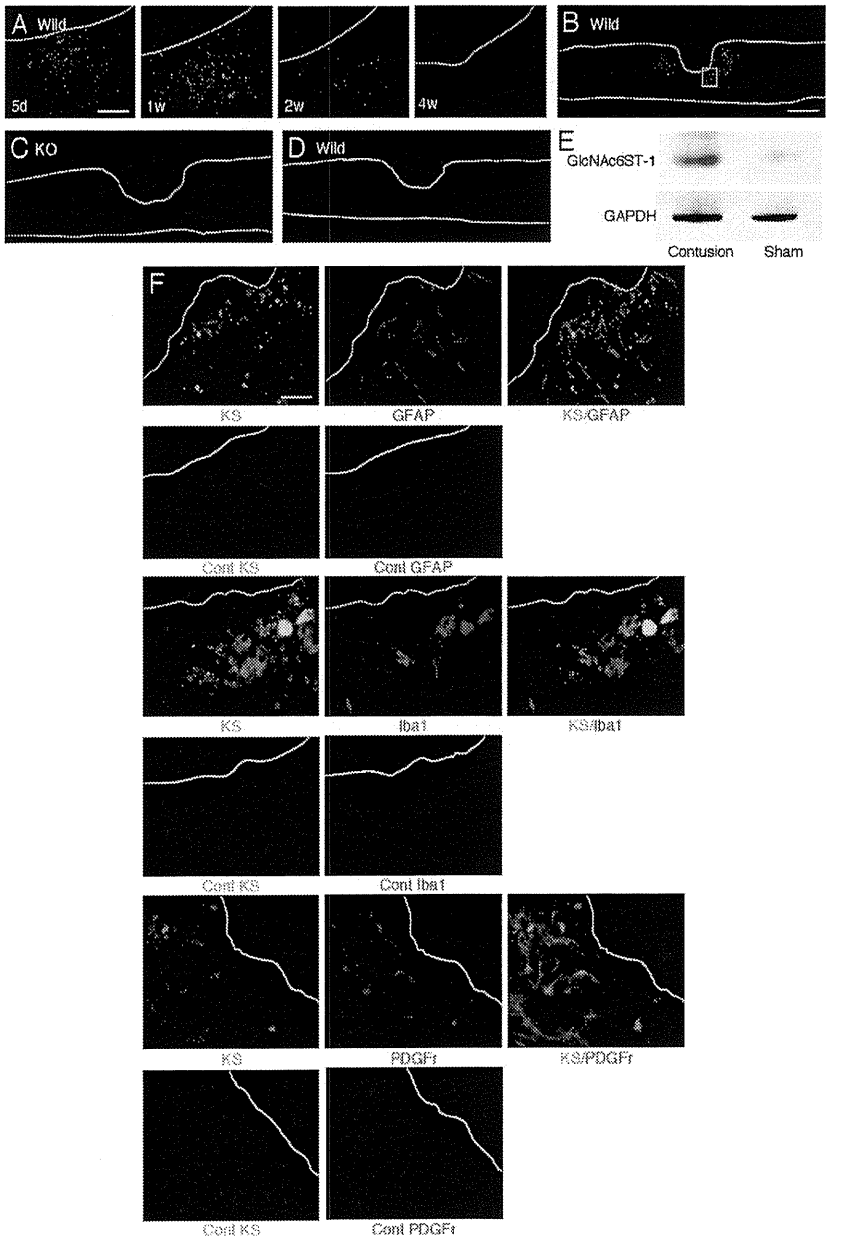

Figure 1. KS expression after spinal cord injury. ***A***, Expression profile of 5D4-reactive KS in wild-type mice after spinal cord injury. Scale bar, 100 μm. d, Day; w, week. ***B–D***, KS was expressed around the lesion center 7 d after injury in wild-type mice (***B***) but was not detected in GlcNAc6ST-1−/− mice (KO; ***C***) or isotype-matched IgG controls (***D***). ***E***, RT-PCR for GlcNAc6ST-1 and GAPDH was performed for samples from the wild-type mouse spinal cord 7 d after injury or sham operation. ***F***, Double staining for KS and a glial cell marker. Reactive astrocytes (GFAP), microglia (Iba1), and oligodendrocyte precursors (PDGF receptors) were examined. Scale bar, 50 μm. The sections shown are midline sagittal sections of the injured spinal cord. The drawn lines indicate the margins of the lesion core (***A***) and the outline of the spinal cord (***B***, ***C***).

vides a gross indication of locomotor ability and determines the phases of locomotor recovery and features of locomotion. The BMS score was determined for seven mice in each group.

Electrophysiology. In terminal electrophysiological experiments, after an intraperitoneal injection of ketamine (100 mg/kg), short trains of five square-wave stimuli of 0.5 ms duration with an interstimulus interval of 2 ms were delivered through the occipito-cervical area by small electrode balls, and needle electrodes were placed in both hindlimbs. The active electrode was placed in the muscle belly, and the reference electrode was placed near the distal tendon of the muscle in each limb. The ground electrode was placed subcutaneously between the coil and the recording electrodes. The onset latency was measured as the length of time in milliseconds between the stimulus and the onset of the first wave. One hundred responses were averaged and stored for off-line analysis of latency.

Cell culture. Sprague Dawley rats at postnatal days 7–9 were killed, and the cerebella were collected. The meninges were carefully removed with fine forceps, and the remaining tissues were minced and digested using a Papain Dissociation System (Worthington). Dissociated cells were applied to a 35/60% two-step Percoll gradient and centrifuged at 3000 × *g* for 15 min. Cerebellar granule neurons at the interface were collected. Cells were suspended in Neurobasal medium (Invitrogen) supplemented with 2% B27 (Invitrogen), 2 mM glutamine, an additional 20 mM KCl, 50 U/ml penicillin, and 50 μg/ml streptomycin.

Substrate preparation. Four-well chamber slides (NUNC) were coated with 20 μg/ml poly-L-lysine (PLL; Sigma) and left overnight at 4°C and then were coated with chick brain proteoglycans (Millipore Bioscience Research Reagents) or the other indicated substrates and left for 4 h at 37°C. If indicated, proteoglycans were treated with 200 mU/ml chondroitinase ABC or 5 mU/ml keratanase II derived from *Bacillus* sp. Ks36 (Seikagaku) in PBS at 37°C. Other substrate materials included poly-L-ornithine, myelin-associated glycoprotein (Sigma), Nogo, oligodendrocyte myelin glycoprotein (R & D Systems), KS and chondroitin sulfate C (Seikagaku).

Cell adhesion assay. Cerebellar granule neurons were seeded onto chick proteoglycan-coated chamber slides at 2.0×10^5 per well. After 2 h, nonadherent cells were washed out with PBS, and adherent cells were visualized by nuclear staining with 4′,6-diamidino-2-phenylindole (DAPI). The number of adherent cells was counted under 200× magnification (six fields).

Neurite outgrowth assays. Cerebellar granule neurons were seeded onto four-well chamber slides at 2.0×10^5 per well. Twenty-four hours after seeding, the neurons were fixed with 4% paraformaldehyde/PBS and stained with anti-neuron-specific β-tubulin (Covance) to visualize neurites. Neurite lengths were measured from at least 100 neurons that had neurites longer than twice the cell body diameter, per condition from duplicate wells, and quantified as described previously (Ughrin et al., 2003).

Isolation and purification of proteoglycans from mouse brains. Whole brains were isolated from C57BL/6J mice (postnatal day 5). Tissues were homogenized in PBS containing 10 mM *N*-ethylmaleimide and protease inhibitor mixtures (Nacalai Tesque) using a Dounce-type homogenizer. Homogenates were centrifuged at 24,000 × *g* for 30 min, and supernatants were applied to DEAE-Sepharose (GE Healthcare). Samples were washed three times with wash buffer (50 mM Tris-HCl, pH 7.5, 2 M urea, 0.25 M NaCl, 20 mM EDTA, 0.2 mM PMSF, 1 mM *N*-ethylmaleimide), and the proteoglycans were eluted with 2 M NaCl. The eluent was concentrated using a size-exclusion spin column (molecular weight cutoff, 100 kDa), and the protein concentration was determined using a Micro BCA Protein Assay kit (Thermo Fisher Scientific).

Spot assay. PLL-coated chamber slides were air dried and spotted with 5 μl of proteoglycans (10 μg/ml) from mouse brains. The spotted area was visualized by staining with rhodamine B (10 μg/ml). If indicated, proteoglycans were predigested with keratanase (500 mU/ml) and keratanase II (5 mU/ml) at 37°C for 2 h before spotting. Cerebellar granule neurons were seeded onto four-well chamber slides at 1.0×10^5 or 1.0×10^6 per well.

Coating efficiency. Five microliters of aggrecan (50 μg/ml), which had been treated with or without keratanase (500 mU/ml) and keratanase II (5 mU/ml) at 37°C for 2 h, were spotted onto PLL-coated chamber slides. After overnight incubation at 37°C, the coated aggrecan was visualized using an anti-CS antibody (CS56), followed by Alexa-488-conjugated anti-mouse IgM antibody.

Statistical analysis. Statistical analyses were performed with an unpaired two-tailed Student's *t* test for single comparisons and one-way ANOVA for multiple comparisons. For the footfall and footprint scores, repeated-measures ANOVA and the Mann–Whitney *U* test were used. In all statistical analyses, values of $p < 0.05$ were considered to indicate significance. To obtain the data for statistical analyses, the investigators were blinded to the genotypes in all procedures.

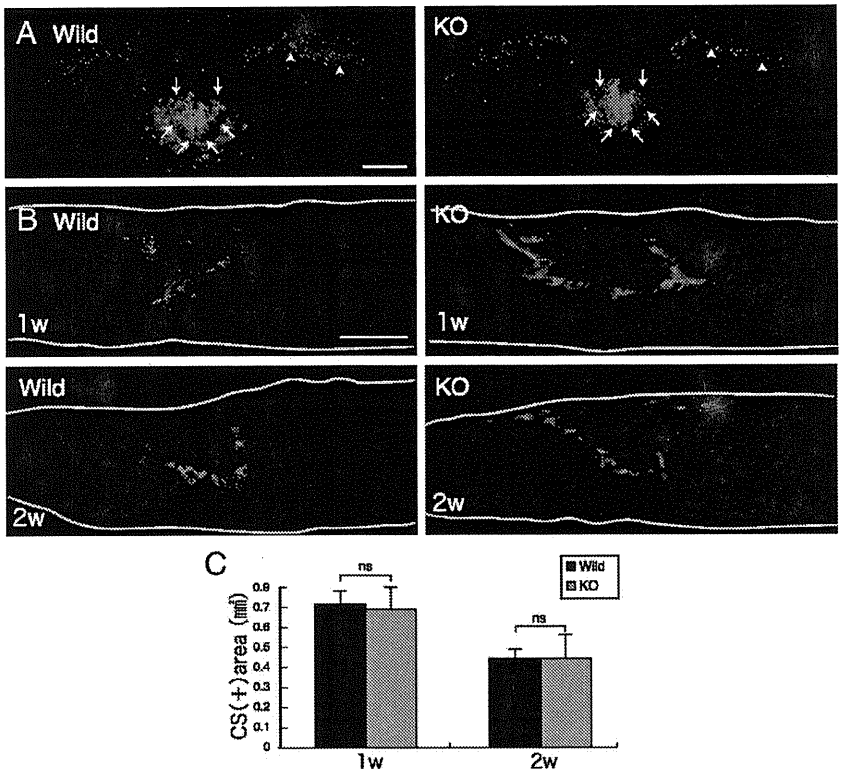

Figure 2. CST and CS expression after injury. ***A***, The CST was stained with anti-protein kinase C-γ antibody (arrow). Densely packed immunofluorescent small cells are located in the inner part of lamina II of the substantia geratinosa (arrowhead) on the axial section. Scale bar, 200 μm. The sections shown are axial sections of the injured spinal cord. ***B***, CS expression was determined with CS-56 antibody. Scale bar, 500 μm. The sections shown are the midline sagittal sections of the injured spinal cord. The drawn lines indicate the outline of the spinal cord. ***C***, Quantification of CS expression. Five mice for each genotype at each time point were examined. Quantification data are the means ± SEM. ns, Not significant (Student's *t* test). w, Week; KO, knock-out.

Results

Induction of KS expression after spinal cord injury in wild-type mice

We used a contusion injury model of the spinal cord to investigate the significance of KS in neurological function after injuries. The contusion injury of the spinal cord was made at the 10th thoracic level with 100 kdyn using an Infinite Horizon Impactor. To reveal the expression and localization of KS, 5D4, an anti-KS monoclonal antibody, was used. 5D4-reactive KS expression was induced around the core lesion, reached a maximum level around 5–7 d after injury in wild-type mice (Fig. 1*A*), and was not detected at all in GlcNAc6ST-1−/− mice (Fig. 1*B–D*). GlcNAc6ST-1 expression was also enhanced in injured wild-type mice (Fig. 1*E*).

Antibodies against GFAP, Iba1, and PDGFr were used to identify KS-expressing cells. 5D4-reactive KS did not overlap GFAP, but a portion of the Iba1-positive cells overlapped 5D4-reactive cells (Fig. 1*F*). Almost all PDGFr-positive cells were 5D4 positive (Fig. 1*F*). These data indicated that KS was mainly expressed by oligodendrocyte precursor cells (PDGFr positive) and partially expressed by microglia (Iba1 positive), which is consistent with the 5D4-reactive KS expression previously reported in a rat spinal cord injury model (Jones and Tuszynski, 2002).

CST, CS expression, and inflammatory cell accumulation

Protein kinase C-γ is a marker for the CST. Protein kinase C-γ immunoreactivity was observed in the dorsal column and lamina II of the spinal cords of uninjured mice (Fig. 2*A*, arrows and arrowheads, respectively) at the T5 level of the cord. The immunoreactivity was similar in wild-type and GlcNAc6ST-1−/− mice (Fig. 2*A*), and the BMS locomotor score before spinal cord injury was also similar in both groups (data not shown), indicating that the CST had formed in a normal fashion in GlcNAc6ST-1−/− mice and thus that these mice could be used for the motor function analyses.

In contrast to KS expression, CS expression in GlcNAc6ST-1−/− mice as judged by CS-56 immunoreactivity was comparable to that in wild-type mice (Fig. 2*B*,*C*). Furthermore, CD11b (a marker of monocytes/macrophages and granulocytes)-positive inflammatory cells were accumulated in the lesion to a similar extent in wild-type and GlcNAc6ST-1−/− mice (data not shown).

Motor function

We next evaluated functional recovery after injury. The footfall test and footprint test were used to objectively evaluate motor function. For the footfall test, mice were placed on a lattice of thin metal wires. This test requires accurate limb placement and precise motor control. Intact animals cross the grid without making footfalls, whereas a paralytic foot tends to fall from the lattice during movement. The numbers of footfalls were comparable between wild-type and GlcNAc6ST-1−/− mice 3 d after injury (Fig. 3*A*). GlcNAc6ST-1−/− mice gradually recovered and, at 4–6 weeks after injury, showed footfall counts comparable to those of sham-operated mice (Fig. 3*A*). In contrast, wild-type mice still showed frequent footfalls at 4 and 6 weeks after injury (Fig. 3*A*; see movie in supplemental Fig. S1, available at www.jneurosci.org as supplemental material).

On the footprint test, GlcNAc6ST-1−/− mice showed a well balanced and organized walk at 4 weeks after injury, whereas wild-type mice showed a disorganized walk, sometimes with toe drop (Fig. 3*B*, arrow). The profiles of stride length deduced

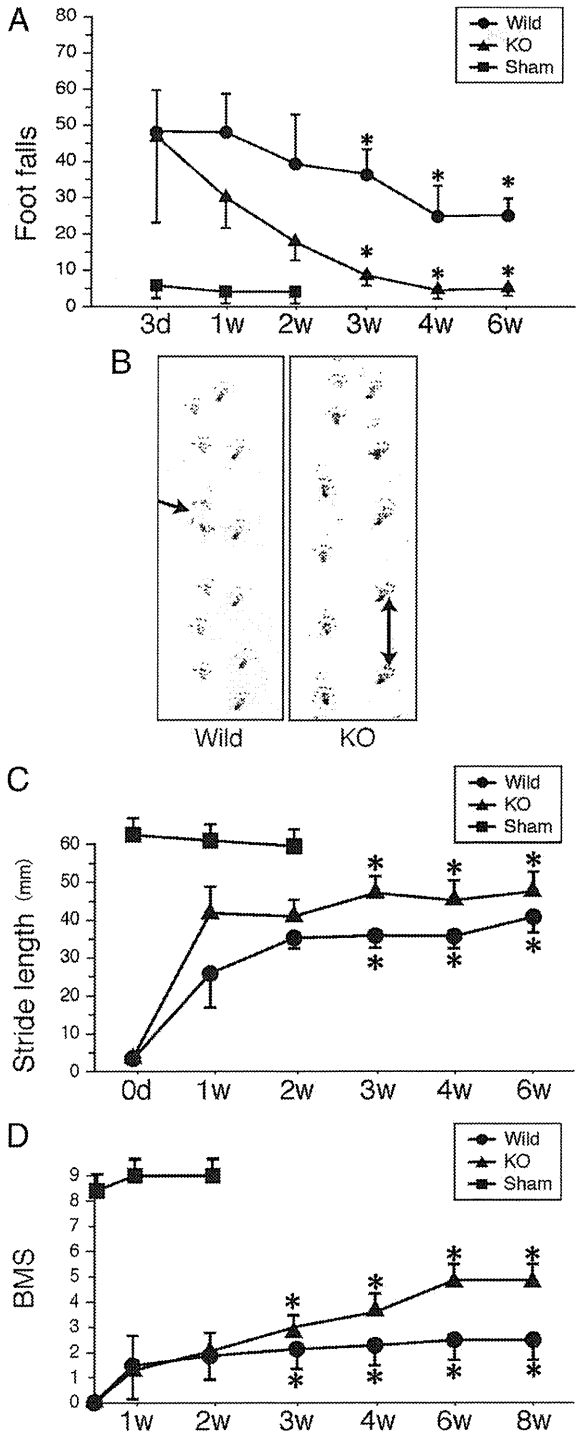

Figure 3. Footfall and footprint tests and BMS scoring. ***A***, Footfall test. The graph shows data from five mice for each genotype at each time point. ***B***, Representative photos of the footprint test taken 4 weeks after injury. The arrow indicates a toe drop. ***C***, Data of the footprint test are quantified. Five mice were used for each genotype at each time point. Quantification data are the means ± SEM (repeated-measures ANOVA and the Mann–Whitney *U* test). ***D***, BMS scoring. The graph shows data from seven mice for each genotype at each time point. $*p < 0.05$ (wild-type vs GlcNAc6ST-1−/− mice). d, Day; w, week; KO, knock-out.

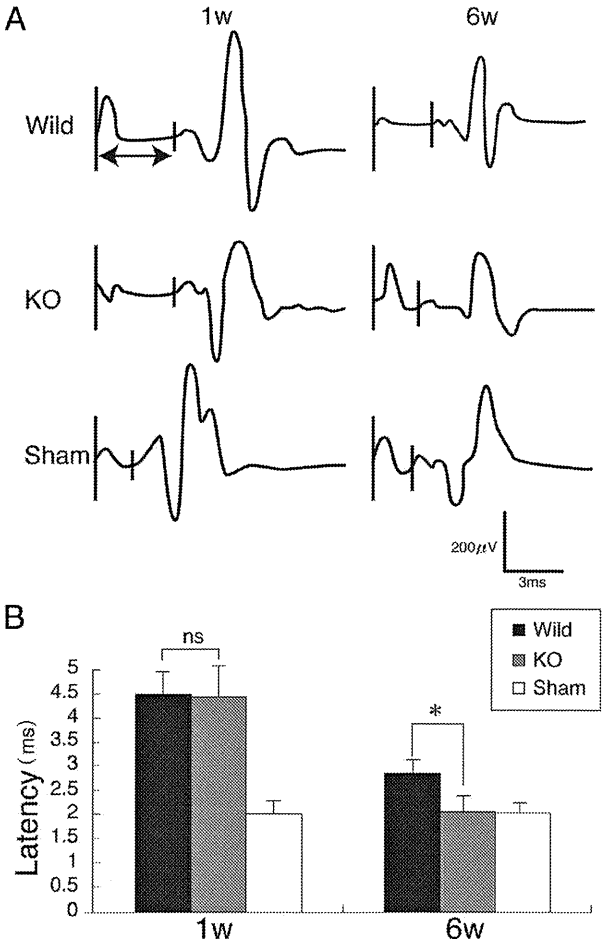

Figure 4. Motor-evoked potential. ***A***, Representative profiles of motor-evoked potentials are shown. ***B***, Latency times were quantified. Five mice were used for each genotype at each time point. $*p < 0.05$. Quantification data are the means ± SEM (one-way ANOVA). W, week; KO, knock-out; ns, not significant.

from the footprints clearly demonstrated that the recovery of motor function was significantly better in GlcNAc6ST-1−/− mice (Fig. 3*C*).

We also performed BMS locomotor scoring for 8 weeks. There was a significantly better recovery in the GlcNAc6ST-1−/− mice than in the wild-type controls (Fig. 3*D*). These data were consistent with those of our footfall scoring and footprints, in which a significant recovery was observed from 3 weeks after the spinal cord injury (Fig. 3*B–D*). Using the same mice as used for BMS scoring, we also examined the footfall test results over a longer period (supplemental Fig. S2 and Table 1, available at www.jneurosci.org as supplemental material) and confirmed the reproducibility of the data in Figure 3*A*. These mice were also compared with hemisection and total section models as described below.

Next, to confirm that our 100 kdyn contusion model inflicted an injury of sufficient severity, we subjected additional mice to total section and hemisection injuries and compared their motor function with that of our 100 kdyn contusion injury model. In the footfall test, the hemisection model showed a substantial degree of spontaneous recovery, reaching an almost normal level 6 weeks after spinal cord injury, whereas the total section model showed a severe motor function disturbance even 6 weeks after injury. The 100 kdyn contusion injury was more severe than the

hemisection injury but milder than the total section injury (supplemental Fig. S2, available at www.jneurosci.org as supplemental material). Furthermore, in the BMS scores of wild-type mice, we did not observe spontaneous recovery of motor function even 8 weeks after contusion injury (Fig. 3*D*). Together, these results suggest that our contusion model was sufficiently severe and was appropriate for evaluating functional recovery after spinal cord injury.

Motor-evoked potential has been widely used in clinical and animal trials of spinal cord injury to evaluate the neuromuscular system function. In the present work, the latency of motor-evoked potential was measured to also objectively evaluate motor function. Mice received electrical stimuli at the occipito-cervical area, and the motor-evoked potential was recorded at both hindlimbs. The latency of the motor-evoked potential was measured from the onset of the stimulus to the first response of each wave. At 1 week after injury, the latency was elongated to a similar extent in wild-type and GlcNAc6ST-1−/− mice, but at 6 weeks after injury, the latency of GlcNAc6ST-1−/− mice became comparable to that of the sham-operated controls, whereas that of wild-type mice was significantly longer (Fig. 4). These data support the conclusion that functional recovery was significantly better in GlcNAc6ST-1−/− mice.

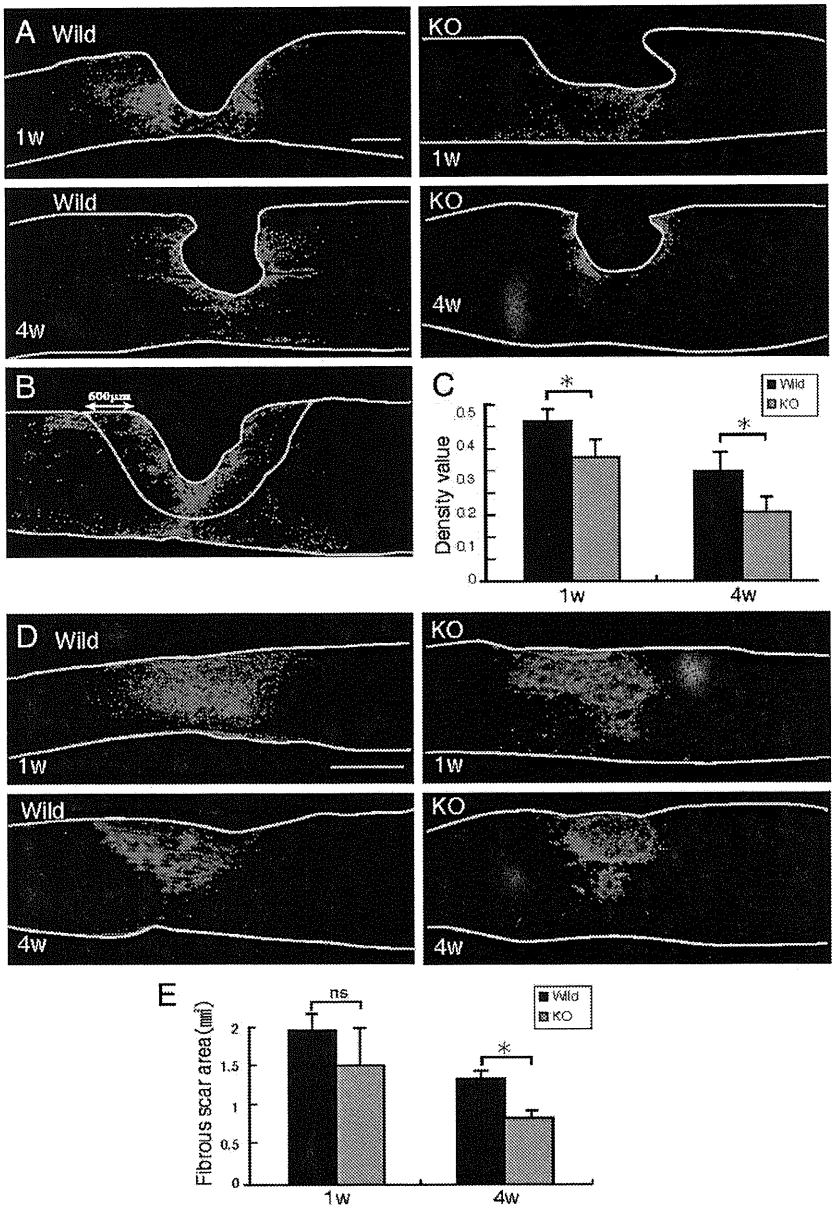

Figure 5. Reactive astrocyte accumulation and collagen IV deposition. ***A***, Representative photos for GFAP expression are shown. Scale bar, 500 μm. The drawn lines indicate the margins of the lesion core and the outline of the spinal cord. ***B***, The GFAP-positive area in a field of 600 μm width around the lesion center (lack of GFAP signal) was measured. The drawn lines indicate the outline of the spinal cord and the measured area. ***C***, The GFAP-positive area is summarized in the graph. Five mice were used for each genotype at each time point. *$p < 0.05$. ***D***, Representative photos for collagen IV expression are shown. Scale bar, 500 μm. The drawn lines indicate the outline of the spinal cord. ***E***, The collagen IV-positive areas are summarized in the graph. Five mice were used for each genotype at each time point. *$p < 0.05$. Quantification data are the means ± SEM (Student's *t* test). The sections shown are midline sagittal sections of the injured spinal cord. W, week; KO, knock-out; ns, not significant.

Glial scar formation

We next examined glial scar formation. Accumulation of GFAP-positive reactive astrocytes appeared after injury in both wild-type and GlcNAc6ST-1−/− mice. However, their accumulation was weaker in GlcNAc6ST-1−/− mice than in wild-type mice: the GFAP-positive area in a region of 600 μm width around the lesion core was significantly smaller in GlcNAc6ST-1−/− mice (Fig. 5*A–C*). An important marker for glial scarring is collagen IV, which appears in the late stages of glial scarring (Liesi and Kauppila, 2002). In the present study, collagen IV expression in the injured area became apparent 7 d after injury in both wild-type and GlcNAc6ST-1−/− mice, but the margin was unclear. There was no difference in scar area (the collagen IV-positive area) between the two genotypes. The margin of the scar area became clear at 4 weeks after injury, and the scar area was significantly reduced in GlcNAc6ST-1−/− mice (Fig. 5*D,E*).

Neuronal axon growth

Regeneration of the serotonergic descending raphespinal tract may partly explain the reason for motor function recovery after spinal cord injury in rodents (Kim et al., 2004). We stained tissues 5 mm distal to the lesion for 5-hydroxytryptamine (5HT), since serotonergic axons are 5HT positive. 5HT-positive fibers were more abundantly found in the ventral horn of the gray matter in GlcNAc6ST-1−/− mice than in wild-type mice (5HT-positive area: wild-type, 972 ± 1080 vs GlcNAc6ST-1−/−, 7120 ± 1168 μm^2; $p < 0.005$) (Fig. 6*A–C*). Positive GAP-43 staining reflects axon regeneration and sprouting (Tetzlaff and Bisby, 1989; King et al., 2001). GAP-43-positive axons were also much more abun-

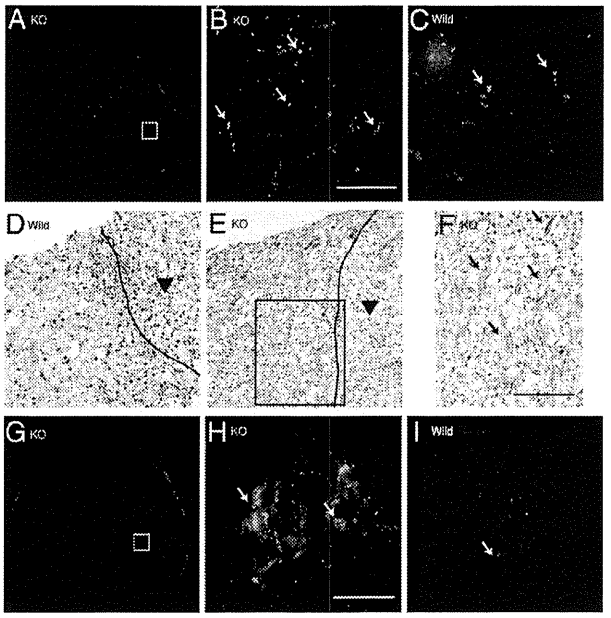

Figure 6. Axonal growth. 5HT staining of the ventral horn (***A–C***; 5 mm distal to the lesion), GAP43 staining (***D–F***), and tracer-fiber counts of the CST (BDA-positive fibers) (***G–I***; 5 mm caudal to the lesion) are shown for GlcNAc6ST-1−/− (***A***, ***B***, ***E–H***) and wild-type (***C***, ***D***, ***I***) mice. Scale bar, 50 μm. Higher-magnification figures of the boxed areas in ***A***, ***E***, and ***G*** are shown in ***B***, ***F***, and ***H***, respectively. The arrows in ***B***, ***C***, ***F***, ***H***, and ***I*** indicate 5HT-, GAP43-, and BDA-positive fibers, respectively. The arrowheads in ***D*** and ***E*** indicate the contusion area. The drawn lines indicate the margins of the lesion core. Five mice were used for each genotype at 4 weeks after injury. The sections in ***A–C***, ***G***, ***H***, and ***I*** are the axial sections of the injured spinal cord. The sections in ***D–F*** are the midline sagittal sections of the injured spinal cord. KO, Knock-out.

dant in GlcNAc6ST-1−/− mice than in wild-type mice at 4 weeks after injury (GAP-43-positive fiber counts/150,000 μm^2: wild-type, 1962 ± 1522 vs GlcNAc6ST-1−/−, 6631 ± 1090; $p < 0.005$) (Fig. 6*D–F*). Moreover, we investigated axonal growth in the CST. In tracer-fiber counts for the CST, the number of BDA-positive fibers was increased in the region caudal to the epicenter in GlcNAc6ST-1−/− mice, particularly in the gray matter in this region (Fig. 6*G–I*). For quantification of the number of labeled BDA, the number of labeled fibers was counted in the gray matter 5 mm caudal to the lesion and divided by the number of labeled corticospinal axons 10 mm rostral to the lesion for each animal. There was a significant difference between wild-type and GlcNAc6ST-1−/− mice (BDA-positive fibers in caudal region/rostral region: wild-type, 1.9 ± 1.1% vs GlcNAc6ST-1−/−, 6.9 ± 1.0%; $p < 0.005$).

Chondroitinase ABC promotes collateral sprouting of spared fibers in the cuneate nucleus after cervical spinal cord injury (Massey et al., 2006), suggesting that proteoglycans limit not only axon regeneration but also sprouting. Our data on 5HT staining, GAP-43 staining, and CST tracer-fiber counts are in line with this idea.

Requirement of KS for the proteoglycan-mediated inhibition of neurite growth

To further explore the underlying mechanisms involving KS in the functional disturbance, we performed *in vitro* experiments. We first asked whether KS was sufficient to inhibit neurite growth. However, glycosaminoglycans (KS and CS), whether administered singly or in combination, did not inhibit neurite outgrowth (Fig. 7*A*). Thus, we focused on the role of KS chains on proteoglycans.

Proteoglycans purified from the brains of chicks contained both KS and CS, because the 5D4-reactive smear appeared more strongly after the CS-degrading enzyme chondroitinase ABC treatment, and the smear disappeared after keratanase II treatment on Western blot analysis (Fig. 7*B*). As it is known that proteoglycans inhibit not only neurite outgrowth but also cell adhesion to the substrate (Kaneko et al., 2007), we examined whether the proteoglycans used in this study would inhibit cell–substrate adhesion. As shown in Figure 7, *C* and *D*, the number of cells adhered to the substrate decreased as the concentration of coated proteoglycans increased. However, if the proteoglycan concentration was lower than 300 ng/ml, the number of cells adhering to the proteoglycans was comparable to the number adhering to the PLL-coated slides (Fig. 7*C*,*D*). Therefore, we decided to use the condition of 300 ng/ml proteoglycans for coating in the neurite outgrowth assay, so that we could discriminate the effect of proteoglycans on neurite outgrowth from that on cell–substrate adhesion.

Proteoglycans coated on the substratum strikingly inhibited the neurite outgrowth of primary neurons compared with the PLL control (Fig. 7*E*,*F*). Molecules derived from myelin, such as Nogo, myelin-associated glycoprotein, and oligodendrocyte-myelin glycoprotein, are known as strong *in vivo* inhibitors of axonal regrowth. Our *in vitro* assay showed that these molecules also inhibit the neurite outgrowth of primary granular neurons from the rat cerebellum (Fig. 7*F*). Notably, the KS-degrading enzyme keratanase II blocked the proteoglycan-mediated inhibition, and this blocking effect was comparable to that of chondroitinase ABC (Fig. 7*E*,*F*).

Finally, we developed an assay system, the spot assay, and used it to examine the activity of mouse brain proteoglycans. We first confirmed that the mouse brain proteoglycans indeed contained both KS and CS (Fig. 8*A*). We then spotted these proteoglycans with rhodamine B, so that the spots appeared red (Fig. 8*B*). Whereas neurites of the primary neurons frequently crossed into the spots in the control (rhodamine B alone) (Fig. 8*B*, top), neurites of neurons in the surrounding area did not enter into the spots of the mouse brain proteoglycans (Fig. 8*B*, middle). However, if the proteoglycans were treated with keratanase, neurites of neurons in the surrounding area could enter the spots (Fig. 8*B*, bottom). This phenomenon was more clearly demonstrated if the seeded cell number was decreased (Fig. 8*C*). Therefore, this *in vitro* assay using brain proteoglycans mimicked the *in vivo* failure of axonal regrowth into the lesions of spinal cord injury and the reversal of this failure in KS-deficient mice.

To examine the possibility that keratanase decreases the efficiency of proteoglycan binding to the substrate, we used the KS/CSPG aggrecan for spotting and visualized spots with the anti-CS antibody CS56. However, we did not observe any difference between spots with and without predigestion with keratanase (supplemental Fig. S3, available at www.jneurosci.org as supplemental material).

Discussion

There have been only a few studies on the relationship between KS and the nervous system. KS expression is induced in the injured CNS after cortical stab wounds in neonatal rats and in the postcomissural fornix after lesioning in adult rats (Geisert and Bidanset, 1993; Stichel et al., 1999). KS expression is also enhanced in reactive microglia and oligodendrocyte progenitors after rat spinal cord injury (Jones and Tuszynski, 2002). After

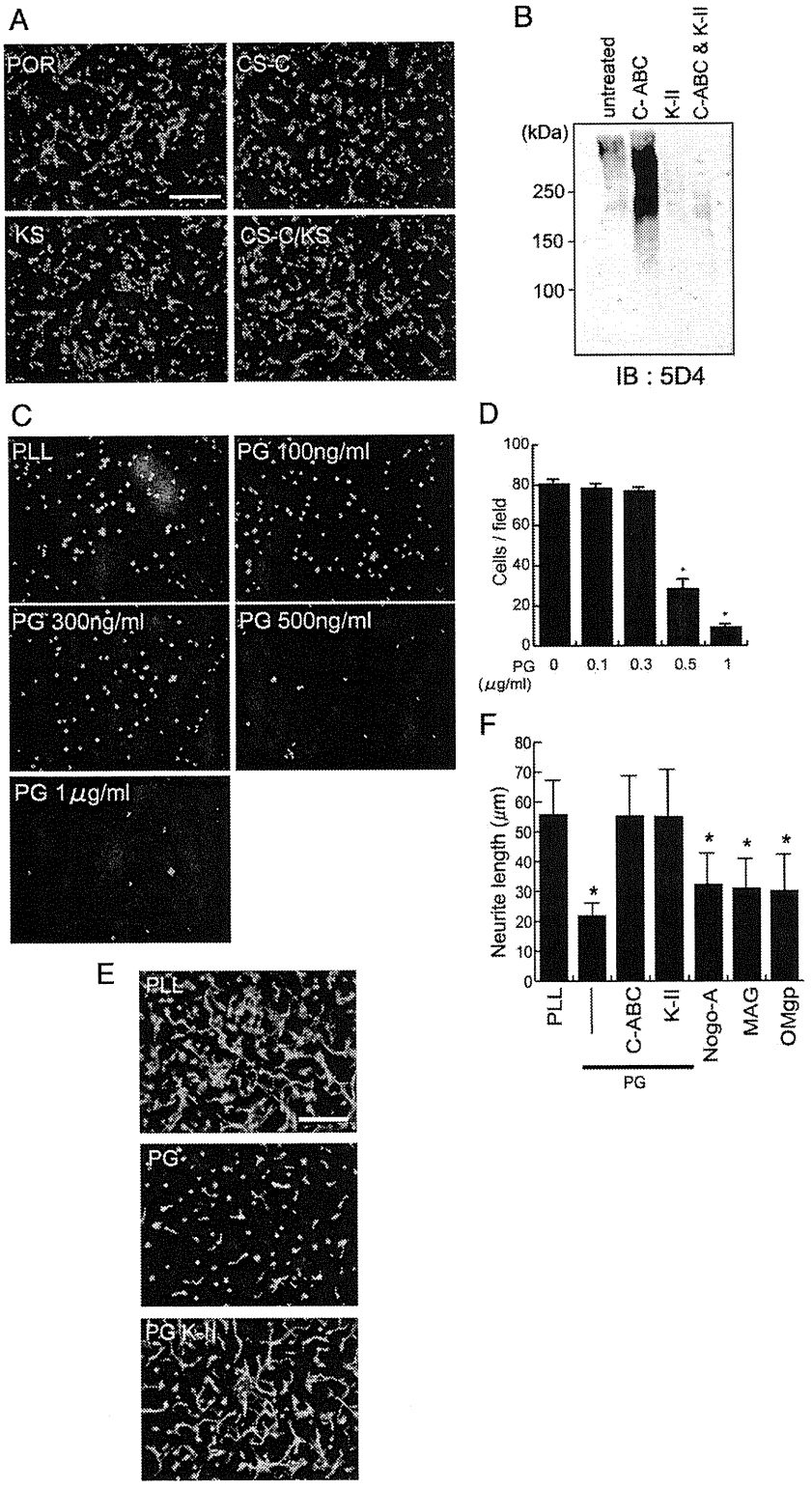

Figure 7. Requirement of KS for the proteoglycan-mediated inhibition of neurite outgrowth. ***A***, Postnatal day 8 (P8) rat cerebellar granule neurons were cultured on poly-L-ornithine (POR), POR plus chondroitin sulfate C (CS-C) (20 μg/ml), or POR plus KS (20 μg/ml). Scale bar, 100 μm. ***B***, Chick brain proteoglycans contained KS. Chick brain proteoglycans (CC117; Millipore) were digested with chondroitinase ABC (C-ABC; 500 mU/ml), keratanase II (K-II; 5 mU/ml), or both and subjected to Western blot analysis. Note that C-ABC treatment revealed KS epitopes. ***C***, P8 rat cerebellar granular neurons were cultured on PLL or proteoglycan (PG) extracted from chick brains. To count adhered cells, the nucleus was stained with DAPI, and the cell number was counted for six fields under 200× magnification. ***D***, The quantification of ***C***. Data represent the average cell number ± SD. *$p <$ 0.01, versus 0 μg of PG. ***E***, P8 rat cerebellar granular neurons were cultured on PLL or PG extracted from chick brains. Keratanase II treatment restored the neurite outgrowth. Scale bar, 100 μm. ***F***, The quantification of ***E***. Data represent the average neurite length ± SD. *$p < 0.05$ versus PLL. PG (300 ng/ml), C-ABC (200 mU/ml), K-II (5 mU/ml), Nogo (800 ng/ml), myelin-associated glycoprotein (MAG) (400 ng/ml), and oligodendrocyte myelin glycoprotein (OMgp) (400 ng/ml) were used.

unilateral axotomy of the nigrostriatal tract in adult rats, CSPGs and keratan sulfate proteoglycans (KSPGs) are predominantly found in the lesion surround where reactive astrocytes, activated microglia, and adult precursor cells are abundant (Moon et al., 2002). We previously found enhanced axonal growth in cortical stab wounds in GlcNAc6ST-1−/− mice, but we were not able to investigate the neurological function of these mice at that time (Zhang et al., 2006). In the present study, GlcNAc6ST-1−/− mice exhibited better motor function recovery and enhanced regeneration of the serotonergic descending raphespinal tract axons and CST axons after spinal cord injury, compared with wild-type mice. In support of these data, we also found that the KS-degrading enzyme keratanase reversed the proteoglycan-mediated inhibition of neurite outgrowth *in vitro*. In light of these results, the present study is the first to demonstrate a possible link between KS and neurological function and indicates that GlcNAc6ST-1−/− mice are a good model for investigating the roles of KS in the CNS.

It is of note that neither CS nor KS was sufficient to inhibit neurite outgrowth *in vitro*. However, CS or KS degradation blocked the inhibitory activity of proteoglycans both from chick brains and mouse brains. These results suggest that KS is required for the proteoglycan-mediated inhibition of neurite outgrowth. To our surprise, the effect of KS degradation on this inhibition was comparable to that of CS degradation. Thus, it will be interesting to ask whether KS degradation also promotes functional recovery after neuronal injuries as CS degradation does.

Among the numerous methods available to assess the recovery of locomotor functions, the Basso, Beattie, and Bresnahan (BBB) locomotor scale is a popular choice, because it measures functional changes in voluntary hindlimb movements. In this study, we first used the BBB locomotor scale using five mice in each group, and although we found a slight difference in recovery between the GlcNAc6ST-1−/− mice and controls, the difference did not reach the level of statistical significance ($p = 0.07$; data not

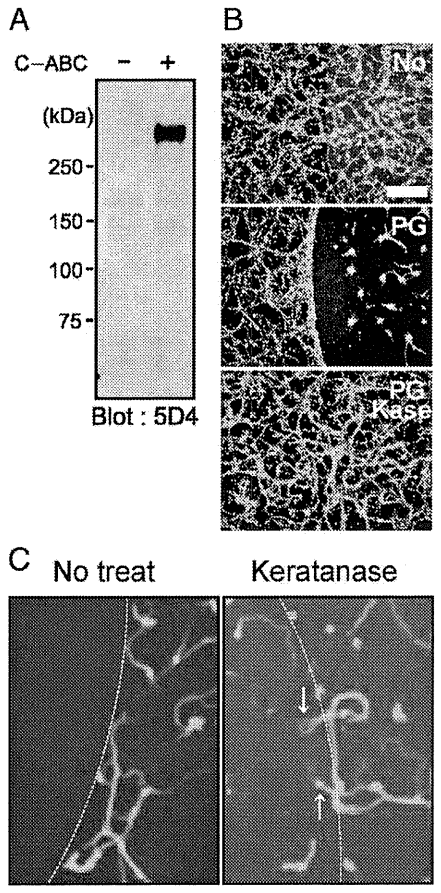

Figure 8. Spot assay. ***A***, Proteoglycans from mouse brain were subjected to Western blot analysis. Note that C-ABC treatment revealed KS epitopes. ***B***, ***C***, Spot assay. Mouse brain proteoglycans at 3 μg/ml were spotted, and primary granular neurons from the rat cerebellum were seeded. Proteoglycans inhibited neurite entry into the spot, whereas keratanase treatment allowed entry. Different cell numbers were used for ***B*** and ***C*** (1.0×10^6 or 1.0×10^5 per well, respectively). Scale bar, 100 μm.

shown). Several locomotor parameters recover differently in mice than in other species (e.g., coordination and paw position recover simultaneously, trunk stability improves earlier, and trunk and hindlimb spasms occur later). These differences limit the sensitivity of the BBB for mice and necessitate a ranking of locomotor attributes unique to mice. To overcome this limitation, a BMS scale was developed for mice (Basso et al., 2006); we applied this locomotor scale using seven mice in each group for 8 weeks and detected a significantly better recovery in the GlcNAc6ST-1−/− mice than in the wild-type controls (Fig. 3*D*). This result was consistent with the footfall, footprint, and motor-evoked potential results. Collectively, the above findings led us to conclude that functional recovery was promoted in GlcNAc6ST-1−/− mice.

The findings of the motor-evoked potential test were consistent with those of the footfall test, footprint test, and BMS scoring. Because the motor-evoked potential test uses only the combination of electric stimulus and response, it can be objectively evaluated. It has recently been shown that motor-evoked potentials have good sensitivity for recording reductions in central conduction latencies (Pluchino et al., 2003; Biffi et al., 2004). In the present study, the responses showed normal configurations, but latency was delayed in the wild-type mice. These electrophysiological data support the idea that the functional recovery of GlcNAc6ST-1−/− mice is remarkably enhanced. However, there may be numerous mechanisms underlying these differences in latency: the conduction differences could be mediated not only by differences in axon regrowth or myelination but also by synaptic reorganization, such as synaptic sprouting, activation of silent synapses, and biochemical synaptic strengthening. Moreover, the type of stimulation used could have activated many descending axon tracts, including not only the CST but also other tracts, such as the rubrospinal, vesitbulospinal, reticulospinal, and propriospinal tracts.

In the present study, we found that most PDGFr-positive cells and a portion of the Iba1-positive cells were KS positive at 7 d after spinal cord injury (Fig. 1). We also found that a portion of the Iba1-positive cells were also KS positive at 3 d, a time point at which most of the Iba1-positive cells were expected to be resident microglia, not macrophages (data not shown). Consistent with this, we have recently reported that primary cultured microglia express KS, and this expression is enhanced by TGF-β, a microglia-activating cytokine usually induced after neuronal injuries (Yin et al., 2009). Considering these results together, it is most likely that, in addition to oligodendrocyte precursor cells (PDGFr positive), activated microglia are a main source of KSPG.

Regarding the reduction of glial scarring in GlcNAc6ST-1−/− mice, whether or not this phenomenon assisted in the functional recovery of these mice is a subject for future debate. Although it is known that glial scars formed in part by reactive astrocytes inhibit axonal sprouting and functional restoration after spinal cord injury (Menet et al., 2003), reactive astrocytes support repair of the blood–brain barrier, prevent inflammatory cell infiltration, and protect neurons and oligodendrocytes (Bush et al., 1999; Faulkner et al., 2004). At least in the subacute phase (within 2 weeks after spinal cord injury), the accumulation of reactive astrocytes helps to repair tissue and restore function (Okada et al., 2006). In this context, our findings are complex. That is, we found that the reactive astrocyte accumulation was significantly lower in GlcNAc6ST-1−/− mice than wild-type mice both at 1 and 4 weeks after injury, whereas the collagen deposition of the GlcNAc6ST-1−/− mice was lower only 4 weeks after injury. It is known that the reactive astrocytes and cells invading into the lesion (i.e., fibroblasts, meningeal cells, and Schwann cells) produce extracellular matrix, including collagen IV (Schwab and Bartholdi, 1996; Fawcett and Asher, 1999; Condic and Lemons, 2002; Buss et al., 2007). However, the influence of collagen IV expression on plasticity and regeneration at the lesion site *in vivo* has been controversial and remains to be elucidated (Shiga and Oppenheim, 1991; Stichel et al., 1999; Weidner et al., 1999; Buss et al., 2007). Thus, our present study has, at least, demonstrated a close association between diminished KS expression and suppressed reactive astrocyte accumulation and collagen IV deposition, although the underlying mechanisms are still elusive.

KS seems to be the most important factor in accounting for the phenotype of GlcNAc6ST-1−/− mice in this study, but we need to exclude the possibility that sulfation modifications on other sugar structures are mediated by GlcNAc6ST-1 and play a role in neuronal function. Other than KS, the only product of GlcNAc6ST-1 thus far identified is sialyl 6-sulfo Le^X, which is a determinant of L-selectin and plays a critical role in lymphocyte recruitment (Uchimura K et al., 2004). GlcNAc sulfation of sialyl 6-sulfo Le^X is mediated either by GlcNAc6ST-1 or -2 (Hemmerich et al., 2001; Uchimura et al., 2004). GlcNAc6ST-1−/− mice show reduced lymphocyte homing to lymph

nodes, and mice doubly deficient in GlcNAc6ST-1 and -2 show significantly greater reduction of lymphocyte homing (Uchimura et al., 2004, 2005; Kawashima et al., 2005). However, we observed a similar degree of CD11b-positive inflammatory cell infiltration in wild-type and GlcNAc6ST-1−/− mice. Therefore, it is not likely that sialyl 6-sulfo Le^X was responsible for the difference in motor function between the wild-type and GlcNAc6ST-1−/− mice in the present study. Furthermore, we obtained evidence that the KS-degrading enzyme keratanase promotes neurite outgrowth, which is inhibited by proteoglycans. Together, our data strongly suggest that the GlcNAc6ST-1 product KS plays a critical role in functional disturbance after spinal cord injury.

References

Akama TO, Nishida K, Nakayama J, Watanabe H, Ozaki K, Nakamura T, Dota A, Kawasaki S, Inoue Y, Maeda N, Yamamoto S, Fujiwara T, Thonar EJ, Shimomura Y, Kinoshita S, Tanigami A, Fukuda MN (2000) Macular corneal dystrophy type I and type II are caused by distinct mutations in a new sulphotransferase gene. Nat Genet 26:237–241.

Basso DM, Fisher LC, Anderson AJ, Jakeman LB, Mctigue DM, Popovich PG (2006) Basso mouse scale for locomotion detects differences in recovery after spinal cord injury in five common mouse strains. J Neurotrauma 23:635–659.

Biffi A, De Palma M, Quattrini A, Del Carro U, Amadio S, Visigalli I, Sessa M, Fasano S, Brambilla R, Marchesini S, Bordignon C, Naldini L (2004) Correction of metachromatic leukodystrophy in the mouse model by transplantation of genetically modified hematopoietic stem cells. J Clin Invest 113:1108–1110.

Borisoff JF, Chan CC, Hiebert GW, Oschipok L, Robertson GS, Zamboni R, Steeves JD, Tetzlaff W (2003) Suppression of Rho-kinase activity promotes axonal growth on inhibitory CNS substrates. Mol Cell Neurosci 2:405–416.

Bradbury EJ, Moon LD, Popat RJ, King VR, Bennett GS, Patel PN, Fawcett JW, McMahon SB (2002) Chondroitinase ABC promotes functional recovery after spinal cord injury. Nature 416:636–640.

Bush TG, Puvanachandra N, Horner CH, Polito A, Ostenfeld T, Svendsen CN, Mucke L, Johnson MH, Sofroniew MV (1999) Leukocyte infiltration, neuronal degeneration, and neurite outgrowth after ablation of scar-forming, reactive astrocytes in adult transgenic mice. Neuron 23:297–308.

Buss A, Pech K, Kakulas BA, Martin D, Schoenen J, Noth J, Brook GA (2007) Growth-modulating molecules are associated with invading Schwann cells and not astrocytes in human traumatic spinal cord injury Brain 130:940–953.

Condic ML, Lemons ML (2002) Extracellular matrix in spinal cord regeneration: getting beyond attraction and inhibition. Neuroreport 13:37–48.

De Winter F, Holtmaat AJ, Verhaagen J (2002) Neuropilin and class 3 semaphorins in nervous system regeneration. Adv Exp Med Biol 515:115–139.

Faulkner RJ, Julia E. Herrmann, Michael J. Woo, Keith E. Tansey, Ngan B. Doan, Michael V. Sofroniew (2004) Reactive Astrocytes Protect Tissue and Preserve Function after Spinal Cord Injury. J Neurosci 24:2143–2155.

Fawcett JW, Asher RA (1999) The glial scar and central nervous system repair. Brain Res Bull 49:377–391.

Filbin MT (2003) Myelin-associated inhibitors of axonal regeneration in the adult mammalian CNS. Nat Rev Neurosci 4:703–713.

Geisert EE Jr, Bidanset DJ (1993) A central nervous system keratan sulfate proteoglycan: localization to boundaries in the neonatal rat brain. Brain Res Dev Brain Res 75:163–173.

Grimpe B, Silver J (2004) Novel DNA enzyme reduces glycosaminoglycan chains in the glial scar and allows microtransplanted dorsal root ganglia axons to regenerate beyond lesions in the spinal cord. J Neurosci 24:1393–1397.

Habuchi H, Habuchi O, Uchimura K, Kimata K, Muramatsu T (2006) Determination of substrate specificity of sulfotransferases and glycosyltransferases (proteoglycans). Methods Enzymol 416:225–243.

Hemmerich S, Bistrup A, Singer MS, van Zante A, Lee JK, Tsay D, Peters M, Carminati JL, Brennan TJ, Carver-Moore K, Leviten M, Fuentes ME, Ruddle NH, Rosen SD (2001) Sulfation of L-selectin ligands by an HEV-restricted sulfotransferase regulates lymphocyte homing to lymph nodes. Immunity 15:237–247.

Jones LL, Tuszynski MH (2002) Spinal cord injury elicits expression of keratan sulfate proteoglycans by macrophages, reactive microglia, and oligodendrocyte progenitors. J Neurosci 22:4611–4624.

Kaneko M, Kubo T, Hata K, Yamaguchi A, Yamashita T (2007) Repulsion of cerebellar granule neurons by chondroitin sulfate proteoglycans is mediated by MAPK pathway. Neurosci Lett 423:62–67.

Kawashima H, Petryniak B, Hiraoka N, Mitoma J, Huckaby V, Nakayama J, Uchimura K, Kadomatsu K, Muramatsu T, Lowe JB, Fukuda M (2005) N-acetylglucosamine-6-O-sulfotransferases 1 and 2 cooperatively control lymphocyte homing through L-selectin ligand biosynthesis in high endothelial venules. Nat Immunol 6:1096–1104.

Kim JE, Liu BP, Park JH, Strittmatter SM (2004) Nogo-66 receptor prevents raphespinal and rubrospinal axon regeneration and limits functional recovery from spinal cord injury. Neuron 44:439–451.

King CE, Canty AJ, Vickers JC (2001) Alterations in neurofilaments associated with reactive brain changes and axonal sprouting following acute physical injury to the rat neocortex. Neuropathol Appl Neurobiol 27: 115–126.

Kitayama K, Hayashida Y, Nishida K, Akama TO (2007) Enzymes responsible for synthesis of corneal keratan sulfate glycosaminoglycans. J Biol Chem 282:30085–30096.

Liesi P, Kauppila T (2002) Induction of type IV collagen and other basement-membrane-associated proteins after spinal cord injury of the adult rat may participate in formation of the glial scar. Exp Neurol 173:31–45.

Massey JM, Hubscher CH, Wagoner MR, Decker JA, Amps J, Silver J, Onifer SM (2006) Chondroitinase ABC digestion of the perineuronal net promotes functional collateral sprouting in the cuneate nucleus after cervical spinal cord injury. J Neurosci 26:4406–4414.

McGee AW, Strittmatter SM (2003) The Nogo-66 receptor: focusing myelin inhibition of axon regeneration. Trends Neurosci 26:193–198.

Menet V, M. Prieto, A. Privat, M. Giménez y Ribotta (2003) Axonal plasticity and functional recovery after spinal cord injury in mice deficient in both glial fibrillary acidic protein and vimentin genes. Proc Natl Acad Sci U S A 100:8999–9004.

Moon LD, Asher RA, Rhodes KE, Fawcett JW (2001) Regeneration of CNS axons back to their target following treatment of adult rat brain with chondroitinase ABC. Nat Neurosci 4:465–466.

Moon LD, Asher RA, Rhodes KE, Fawcett JW (2002) Relationship between sprouting axons, proteoglycans and glial cells following unilateral nigrostriatal axotomy in the adult rat. Neuroscience 109:101–117.

Mueller BK, Mack H, Teusch N (2005) Rho kinase, a promising drug target for neurological disorders. Nat Rev Drug Discov 4:387–398.

Neumann S, Woolf CJ (1999) Regeneration of dorsal column fibers into and beyond the lesion site following adult spinal cord injury. Neuron 23:83–91.

Okada S, Nakamura M, Katoh H, Miyao T, Shimazaki T, Ishii K, Yamane J, Yoshimura A, Iwamoto Y, Toyama Y, Okano H (2006) Conditional ablation of Stat3 or Socs3 discloses a dual role for reactive astrocytes after spinal cord injury. Nat Med 12:829–834.

Pluchino S, Quattrini A, Brambilla E, Gritti A, Salani G, Dina G, Galli R, Del Carro U, Amadio S, Bergami A, Furlan R, Comi G, Vescovi AL, Martino G (2003) Injection of adult neurospheres induces recovery in a chronic model of multiple sclerosis. Nature 422:688–694.

Ruoslahti E (1996) Brain extracellular matrix. Glycobiology 6:489–492.

Schwab ME (2004) Nogo and axon regeneration. Curr Opin Neurobiol 14:118–124.

Schwab ME, Bartholdi D (1996) Degeneration and regeneration of axons in the lesioned spinal cord. Physiol Rev 76:319–370.

Shiga T, Oppenheim RW (1991) Immunolocalization studies of putative guidance molecules used by axons and growth cones of intersegemental interneurons in the chick embryo spinal cord. J Comp Neurol 310:234–252.

Silver J, Miller JH (2004) Regeneration beyond the glial scar. Nat Rev Neurosci 5:146–156.

Stichel CC, Hermanns S, Luhmann HJ, Lausberg F, Niermann H, D'Urso D, Servos G, Hartwig HG, Müller HW (1999) Inhibition of collagen IV deposition promotes regeneration of injured CNS axons. Eur J Neurosci 11:632–646.

Tetzlaff W, Bisby MA (1989) Neurofilament elongation into regenerating facial nerve axons. Neuroscience 29:659–666.

Uchimura K, Kadomatsu K, El-Fasakhany FM, Singer MS, Izawa M, Kannagi R, Takeda N, Rosen SD, Muramatsu T (2004) N-acetylglucosamine 6-O-sulfotransferase-1 regulates expression of L-selectin ligands and lymphocyte homing. J Biol Chem 279:35001–35008.

Uchimura K, Gauguet JM, Singer MS, Tsay D, Kannagi R, Muramatsu T, von Andrian UH, Rosen SD (2005) A major class of L-selectin ligands is eliminated in mice deficient in two sulfotransferases expressed in high endothelial venules. Nat Immunol 6:1105–1113.

Ughrin YM, Chen ZJ, Levine JM (2003) Multiple regions of the NG2 proteoglycan inhibit neurite growth and induce growth cone collapse. J Neurosci 23:175–186.

Weidner N, Grill RJ, Tuszynski MH (1999) Elimination of basal lamina and the collagen "scar" after spinal cord injury fails to augment corticospinal tract regeneration. Exp Neurol 160:40–50.

Widenfalk J, Lundströmer K, Jubran M, Brene S, Olson L (2001) Neurotrophic factors and receptors in the immature and adult spinal cord after mechanical injury or kainic acid. J Neurosci 21:3457–3475.

Yin J, Sakamoto K, Zhang H, Ito Z, Imagama S, Kishida S, Natori T, Sawada M, Matsuyama Y, Kadomatsu K (2009) Transforming growth factor-beta1 upregulates keratan sulfate and chondroitin sulfate biosynthesis in microglia after brain injury. Brain Res 1263:10–22.

Zhang H, Muramatsu T, Murase A, Yuasa S, Uchimura K, Kadomatsu K (2006) N-Acetylglucosamine 6-O-sulfotransferase-1 is required for brain keratan sulfate biosynthesis and glial scar formation after brain injury. Glycobiology 16:702–710.

Development/Plasticity/Repair

Keratan Sulfate Restricts Neural Plasticity after Spinal Cord Injury

Shiro Imagama,[1,2]* Kazuma Sakamoto,[1]* Ryoji Tauchi,[2] Ryuichi Shinjo,[2] Tomohiro Ohgomori,[1] Zenya Ito,[1,2] Haoqian Zhang,[1,3] Yoshihiro Nishida,[2] Nagamasa Asami,[4] Sawako Takeshita,[4] Nobuo Sugiura,[5] Hideto Watanabe,[5] Toshihide Yamashita,[6] Naoki Ishiguro,[2] Yukihiro Matsuyama,[2,7] and Kenji Kadomatsu[1]

Departments of [1]Biochemistry and [2]Orthopedics, Nagoya University Graduate School of Medicine, Showa-ku, Nagoya 466-8550, Japan, [3]Department of Neurosurgery, University of California, San Francisco, California 94143-0110, [4]Central Research Laboratories, Seikagaku Corporation, Higashiyamato, Tokyo 207-0021, Japan, [5]Institute for Molecular Science of Medicine, Aichi Medical University, Yazako, Nagakute, Aichi 480-1195, Japan, [6]Department of Molecular Neuroscience, Graduate School of Medicine, Osaka University, Suita, Osaka 565-0871, Japan, and [7]Department of Orthopedics, Hamamatsu University School of Medicine, Hamamatsu 431-3192, Japan

Chondroitin sulfate (CS) proteoglycans are strong inhibitors of structural rearrangement after injuries of the adult CNS. In addition to CS chains, keratan sulfate (KS) chains are also covalently attached to some proteoglycans. CS and KS sometimes share the same core protein, but exist as independent sugar chains. However, the biological significance of KS remains elusive. Here, we addressed the question of whether KS is involved in plasticity after spinal cord injury. Keratanase II (K-II) specifically degraded KS, i.e., not CS, *in vivo*. This enzyme digestion promoted the recovery of motor and sensory function after spinal cord injury in rats. Consistent with this, axonal regeneration/sprouting was enhanced in K-II-treated rats. K-II and the CS-degrading enzyme chondroitinase ABC exerted comparable effects *in vivo* and *in vitro*. However, these two enzymes worked neither additively nor synergistically. These data and further *in vitro* studies involving artificial proteoglycans (KS/CS-albumin) and heat-denatured or reduced/alkylated proteoglycans suggested that all three components of the proteoglycan moiety, i.e., the core protein, CS chains, and KS chains, were required for the inhibitory activity of proteoglycans. We conclude that KS is essential for, and has an impact comparable to that of CS on, postinjury plasticity. Our study also established that KS and CS are independent requirements for the proteoglycan-mediated inhibition of axonal regeneration/sprouting.

Introduction

The CNS extracellular matrix (ECM) may play a role in the maintenance of the neuronal network by inhibiting axonal growth and suppressing the formation of additional inadequate synapses. Upon neuronal injury, disorganized production of proteoglycans in the ECM is initiated, leading to the inhibition of structural rearrangement of the neuronal network. Among proteoglycans, chondroitin sulfate proteoglycans (CSPGs) have received particular attention; dystrophic end balls end in the CSPG deposition area at the injury site (Davies et al., 1999; Grimpe and Silver, 2004; Silver and Miller, 2004; Tom et al., 2004), and CSPGs inhibit neurite outgrowth *in vitro*. The chondroitin sulfate (CS)-degrading enzyme chondroitinase ABC (C-ABC) promotes axonal regeneration after nigrostriatal tract transaction (Moon et al., 2001), collateral sprouting of spared fibers in the cuneate nucleus after cervical spinal cord injury (SCI) (Massey et al., 2006), and functional recovery after SCI (Bradbury et al., 2002). Thus, the CS chains of the CSPG moiety seem to be principal for the CSPG-mediated inhibition of structural rearrangement.

Proteoglycans consist of a core protein and covalently attached long sugar chains of repeating disaccharide units with sulfation, or so-called glycosaminoglycans (GAGs). Four sulfated glycosaminoglycans are known, i.e., CS, dermatan sulfate, heparan sulfate, and keratan sulfate (KS). Most proteoglycans carry a single glycosaminoglycan (such as a CSPG or KSPG), but a few proteoglycans, e.g., aggrecan (KS/CSPG), have two types of glycosaminoglycan.

KS is expressed in the rodent roof plate of the spinal cord, and is induced after SCI and injury in the brain (Snow et al., 1990a; Cole and McCabe, 1991; Geisert et al., 1996; Jones and Tuszynski, 2002; Krautstrunk et al., 2002; Moon et al., 2002). *In vitro* digestion of KS restores neurite outgrowth on proteoglycan-coated substratum (Snow et al., 1990b; Powell et al., 1997). Thus, KS has been implicated in the regulation of axon guidance and/or axonal regeneration/sprouting. However, its biological impact on neu-

Received Sept. 29, 2010; revised Sept. 6, 2011; accepted Oct. 1, 2011.

Author contributions: S.I., H.Z., Y.N., N.A., S.T., N.S., H.W., T.Y., N.I., Y.M., and K.K. designed research; S.I., K.S., R.T., and R.S. performed research; S.I., T.O., Z.I., and K.K. analyzed data; S.I. wrote the paper.

This work was supported in part by a Grant-in-Aid for Scientific Research on Innovative Areas (No. 23110002 to K.K.) from Ministry of Education, Culture, Sports, Science, and Technology (MEXT), Japan; by Grants-in-Aid for Scientific Research (Nos. 18390099 and 20390092 to K.K.) from MEXT, Japan; by the Ministry of Health, Labor, and Welfare of Japan (Health Sciences Research Grant on Comprehensive Research on Disability Health and Welfare, H21-012 to K.K.); and by funds from the Global Centers of Excellence program, MEXT, Japan, to Nagoya University. We thank K. Suzuki, Y. Kurahashi, and A. Tanaka (Seikagaku Corporation) for performing the stability test of K-II and the HPLC analysis of sugar, M. Sawada (Nagoya University) for guidance with the primary culture of neurons, and N. Ozaki (Nagoya University) for guidance with the sensory tests. We also thank T. Natori (Yamanashi-Gakuin University) and M. Iida, Y. Naito, S. Nakashima, N. Misawa, and Y. Miwa (Nagoya University) for their excellent technical assistance.

*S.I. and K.S. contributed equally to this work.

Correspondence should be addressed to Kenji Kadomatsu, Department of Biochemistry, Nagoya University Graduate School of Medicine, 65 Tsurumai-cho, Showa-ku, Nagoya 466-8550, Japan. E-mail: kkadoma@med.nagoya-u.ac.jp.

DOI:10.1523/JNEUROSCI.5120-10.2011

 0270-6474/11/3117091-12$15.00/0

ronal injuries and the underlying mechanisms have been poorly studied. We have recently found that mice deficient in the enzyme *N*-acetylglucosamine 6-*O*-sulfotransferase-1 lose reactivity to the anti-KS antibody 5D4 in the brain, and show better axonal growth than wild-type mice after a cortical stab wound (Zhang et al., 2006). We have also found that the mice deficient in this enzyme show better motor function recovery and enhanced axonal regeneration/sprouting after SCI (Ito et al., 2010). However, as these knock-out mice lose *N*-acetylglucosamine 6-*O*-sulfotransferase-1 in every cell in the body, critical questions remain to be answered, e.g., whether KS specifically works in the spinal cord, and how much impact KS has on functional disturbance. Furthermore, with regard to the functional redundancy between CS and KS, it is also an important question whether KS collaborates with CS, or works independently.

In the present study, we used keratanase II (K-II), which specifically degrades KS, and investigated the role of KS in postinjury plasticity. We found that KS and CS have a comparable impact on this form of plasticity. We also determined the structural basis of proteoglycan-mediated inhibition of neural plasticity.

Materials and Methods

Surgical procedure. Adult female Sprague Dawley rats weighing 200–230 g were used in the study of SCI. The animals were anesthetized with an intraperitoneal injection of ketamine (100 mg/kg) and xylazine (10 mg/kg). After Th9 laminectomy, we exposed the dura mater and induced injury using a force of 200 kdyn using a commercially available SCI device (Infinite Horizon Impactor; Precision Systems and Instrumentation) that provided a consistent degree of spinal cord contusion injury. All injuries included the dorsal CST and dorsal gray matter. Immediately after the spinal cord contusion, we performed a Th12 partial laminectomy, inserted a thin silicone tube with an osmotic mini-pump into the subarachnoid cavity, and set the tube tip at the Th9 level under a surgical microscope. This tube was very soft and thin so that we could minimize damage to the spinal cord. The osmotic mini-pumps (200 μl of solution, 0.5 μl/h, 14 d delivery; Alzet pump model 2002 [Durect]) were filled with K-II (0.05 U/200 μl; purified from *Bacillus circulans*) (Yamagishi et al., 2003), C-ABC (0.05 U/200 μl) (Seikagaku), or saline (as a vehicle control). To determine an appropriate dose of C-ABC, we examined several doses and found that at the doses of 0.05, 0.1, and 1.0 U/200 μl, C-ABC showed a comparable effect on motor function recovery, while the dose of 0.025 U/200 μl showed a less potent effect (supplemental Fig. 1, available at www.jneurosci.org as supplemental material). Therefore, we used 0.05 U/200 μl of C-ABC in this study.

The tube was sutured to the spinous process to anchor it in place, and the mini-pump was placed under the skin on the animal's back. Afterward, the muscles and skin were closed in layers. The bladder was compressed by manual abdominal pressure twice a day until bladder function was restored. Food was provided on the cage floor, and the rats had no difficulty reaching their water bottles. All animals were given antibiotics in their drinking water [1.0 ml of Bactramin (Roche) in 500 ml of acidified water] for 2 weeks after SCI. We excluded the rats without complete paraplegia on the next day after operation in all groups as they were inappropriate for further evaluation. Although the number of such rats was very small (~1 of 70 rats after injury with our hands), we consistently found that rats without complete paraplegia showed a histology of incomplete injury of the spinal cord. However, no rats were excluded from any groups thereafter, with the exception of rats that had died. We performed postmortem histological measurement and found that all the dead rats had complete severe injury in the spinal cord (data not shown). Therefore, it was not likely that rats with serious spinal shock but minor injury were involved in the experiments in the current study. The number of rats undergoing operation and the number of rats evaluated in each experiment are summarized in Table 1. All animals were treated and cared for in accordance with the Nagoya University School of Medicine Guidelines pertaining to the treatment of experimental animals.

Basso, Beattie, and Bresnahan open field locomotor test. The recovery of hindlimb motor function was assessed by determining the Basso, Beattie, and Bresnahan (BBB) scores (Basso et al., 1995). The results were quantified in a blinded manner by two observers.

Table 1. Number of rats undergoing operation and evaluated in each experiment

Models	Rats	
	Number used for operation	Final number evaluated
EXP1: concentration (Fig. 2*D*,*E*)		
K-II 0.05 U	10	7
K-II 0.005 U (1/10)	10	5
K-II 0.000025 U (1/2000)	10	6
K-II (heat-denatured)	10	5
Vehicle	10	7
EXP2: functional recovery (Fig. 2*A*,*B*)		
K-II 0.05 U	12	10
C-ABC	12	7
Vehicle	12	10
EXP3: functional recovery (Fig. 2*F*)		
Vehicle	12	9
C-ABC	12	7
K-II	12	11
K-II + C-ABC	12	7
EXP4: MEP (Fig. 2*C*)		
Sham	10	8
Vehicle	10	9
C-ABC	10	5
K-II	10	7
K-II + C-ABC	10	7

EXP, Experiment.

%Grip test. Paw placement for each limb on the grid bar was assessed as the animal walked on a plastic-coated wire mesh grid (50 cm length × 33 cm width × 20 cm height, with 2.5 × 2.5 cm openings) for 3 min. Steps in which the paw gripped the grid bar and supported the animal's weight were counted as correct. The number of correct paw placements was expressed as a percentage of the total steps. The percentage of correct paw placements was calculated for each hindlimb and averaged.

Touch test. A touch test was performed preoperatively and then weekly after the operation. Rats were habituated for 30 min in elevated clear plastic cages with wire mesh grid floors. Graded von Frey hair (vFH) monofilaments were applied to the plantar surface of the foot, ~1 cm posterior to the footpad of the middle phalange with the up-down method using procedures described in detail previously (Hutchinson et al., 2004).

Testing began with 15.14 g vFH applied to the hindpaw and continued until 10 trials per hindpaw were completed. Rats were given a food reward throughout testing to prevent visual recognition of the application of the monofilament. A trial was discarded and reperformed if vFH application lifted the paw, producing proprioceptive rather than tactile input. A positive response occurred when the paw was briskly withdrawn from the monofilament. The lowest gram force that produced withdrawal was designated as the response threshold. The thresholds of the bilateral hindpaws were averaged. It was previously determined that the average vFH hindpaw threshold in normal rats is 60 g; in the present study, therefore, we preoperatively excluded rats with a vFH threshold higher than this value. The examiners were blind to group assignment during the vFH testing.

Tail-immersion test. The tail-immersion test was used to determine the somatic thermo-threshold of rats preoperatively and then weekly after the operation. Briefly, rats were gently lifted from their home cages and taken to the test room, where the withdrawal latency of the tail to a temperature stimulus was measured by immersing the tail in a 55 ± 0.5°C water bath. The cutoff time was set at 8 s to avoid skin damage. Rats underwent this test three times at intervals of 15 min. The measurements were averaged to obtain the withdrawal latency time in seconds. Between sessions, the rats were returned to their home cages. Based on the results, we preoperatively excluded rats with prolonged withdrawal latency. Examiners were blind to the group assignment during the tail-immersion test.

Western blotting. The 10-mm-long sections of the injured spinal cord at 1 week after SCI were dissected and homogenized in PBS including 1%

Table 2. Purification of keratanase II

Step	Enzyme activity (units)		
	BcKeratanase	Chondroitinase	α-Galactosidase
Cell extract	38.000	7.000	12.000
Salting out	33.060	3.500	3.960
Desalting	29.260	3.150	3.600
DEAE-cellulose	20.900	0.013	2.400
Phenyl-sepharose	20.900	0.000	0.000

Keratanase unit: One unit will liberate 1.0 μmol of reducing sugar as 2-acetamido-2- deoxy-D-glucose from keratan sulfate per minute at pH 6.0 at 37°C. Chondroitinase unit: One unit will liberate 1.0 μmol of 2-acetamido-2-deoxy-3-*O*-(β-D-gluc-4-ene-pyranosyluronic acid)-6-*O*-sulfo-D-galactose from chondroitin sulfate C per minute at pH 8.0 at 37°C. α-Galactosidase unit: One unit will hydrolyze 1.0 μmol of *p*-nitrophenyl-α-D-galactopyranoside per minute at pH 6.5 at 37°C.

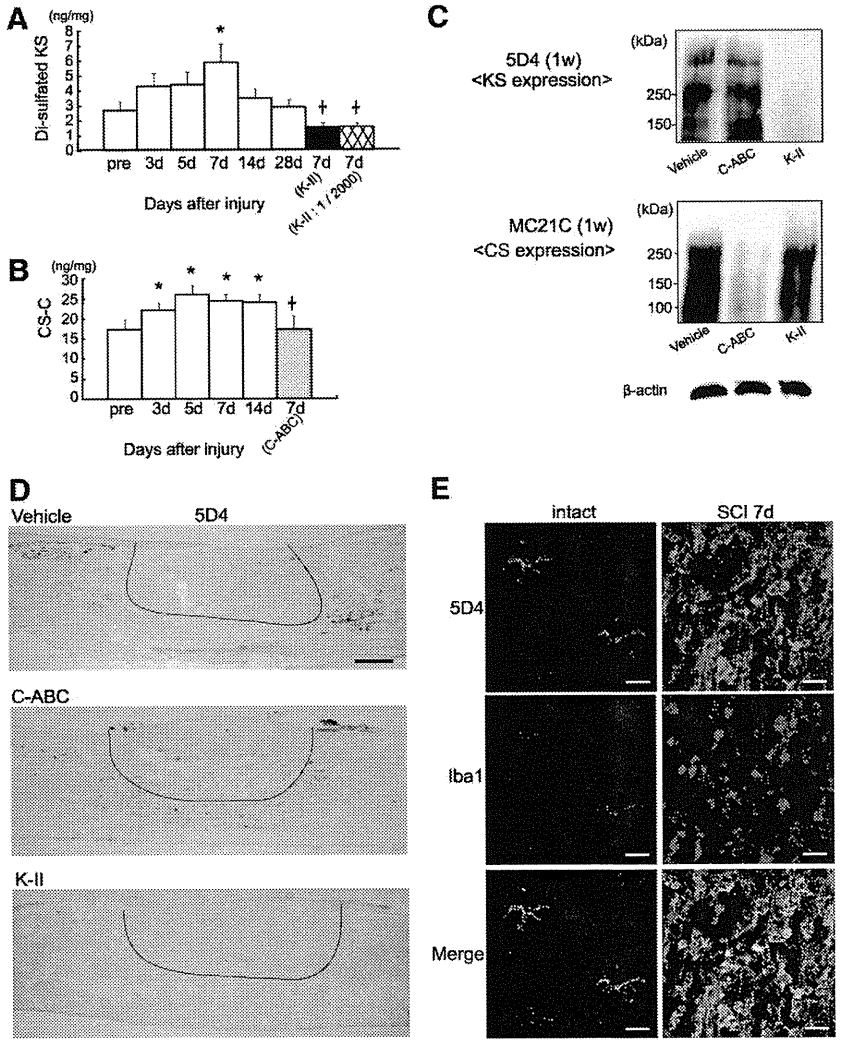

Figure 1. Specific degradation of KS by K-II. ***A***, Amounts of disulfated KS after SCI. A 10 mm fragment of the injured spinal cord was subjected to the analysis. Data represent the means ± SEM. $*p < 0.05$ versus the preinjured specimen (pre). $^{+}p < 0.05$ versus 7 d; $n = 5$ in each group. K-II, 0.05 U of K-II was administered to the spinal cord; K-II 1/2000, 0.0000025 U of K-II was administered to the spinal cord. ***B***, Amounts of CS-C after SCI. $*p < 0.05$ versus pre; $^{+}p < 0.05$ versus 7 d; $n = 6$ in each group. C-ABC, 0.05 U of C-ABC was administered to the spinal cord. ***C***, Rats were treated with K-II or C-ABC for 1 week after spinal cord injury. A 10 mm specimen of the injured spinal cord was subjected to Western blot analysis for 5D4-reactive KS, MC21C-reactive CS, and β-actin. ***D***, 5D4-reactive KS was visible in the penumbra region in vehicle- and C-ABC-treated rats, but not in K-II-treated rats. These rats were treated with the indicated enzyme for 1 week after spinal cord injury. Scale bars, 500 μm. All photos are of sagittal sections with the left side rostral. ***E***, Double staining for KS (5D4) and microglia (Iba1). The left panels show the intact spinal cord, and the right panels show the spinal cord 1 week after injury. Most 5D4-reactive cells overlapped Iba1-positive cells, which indicated that KS was mainly expressed by microglia. The left images showed ramified microglia expressing 5D4-KSPG. The right images show that 5D4-KSPG expression is seen on characteristic cellular profiles with short processes and a less ramified morphology after SCI. Scale bars, 20 μm.

Triton X-100 and protease inhibitors solution (Sigma). Samples of the supernatant fraction were collected after centrifuging at 10,000 × *g* for 30 min. Thirty microliters of each sample was applied and separated by electrophoresis on 6% SDS-PAGE. Proteins were then blotted onto nitrocellulose membranes. Blots were blocked with 5% fat-free dry milk in PBS for 60 min and incubated overnight at 4°C with the primary antibody anti-KS 5D4 (1 μg/ml; Seikagaku) or anti-CS MC21C (1 μg/ml; Seikagaku) in PBS containing 0.3% Triton X-100, washed, and then incubated with a second antibody, HRP-conjugated goat anti-mouse IgM (1/5000; Southern Biotechnology), at room temperature for 60 min. Anti-β-actin antibody (1/100,000; Sigma) was also used as indicated. Bound antibodies were visualized with an ECL-plus Western blotting detection kit (GE Healthcare).

Immunohistochemistry and immunocytochemistry. After terminal anesthesia by ether hyperaspiration, rats were perfused transcardially with buffered 4% paraformaldehyde. The spinal cords and brains were removed, postfixed overnight, and then cryoprotected in buffered 30% sucrose the next night. Tissues were cut into 20 μm sections with a cryostat and mounted on glass slides. The sections were blocked in PBS containing 3% BSA and 5% normal mouse serum for staining of biotin-conjugated anti-KS 5D4 or blocked in PBS containing 1% BSA and 10% normal goat serum for other immunohistochemistry. The sections were then incubated with the primary antibodies to KS (5D4; Seikagaku), Iba1 (Wako Pure Chemical Industries), GAP-43 (Millipore), serotonin (5-HT, Immunostar), type IV collagen (LSL), and GFAP (Sigma). After rinsing, the sections were incubated with the secondary antibody for 60 min at room temperature: Cy3- or Cy2-conjugated streptavidin (Jackson ImmunoResearch), Cy3-conjugated goat anti-rabbit IgG (Zymed Laboratories), Cy3-conjugated goat anti-mouse IgM (Jackson ImmunoResearch), FITC-conjugated goat anti-rat IgG (Sigma), and Alexa Fluor 488 goat anti-mouse IgG (Invitrogen). Sections were then rinsed, mounted with FluorSave (Calbiochem), and examined by confocal microscopy (MRC 1024; Bio-Rad Laboratories).

Morphometry. The extent of axonal outgrowth of each wound area was assessed by counting signals visualized on staining with GAP-43 and 5-HT using serial sagittal 20 μm sections. Morphometry analysis was performed using a computer-driven microscope stage (MetaMorph Offline, version 6.3r^2; Molecular Devices Corporation). In all sagittal sections shown here, the left side is rostral.

Anterograde labeling of the corticospinal tract. Eight weeks after injury, descending corticospinal tract (CST) fibers were labeled with biotin-dextran amine (BDA; 10% in saline, 3.5 μl per cortex, molecular weight 10,000; Invitrogen) injected under anesthesia into the left and right motor cortices (coordinates, 2 mm posterior and 2 mm lateral to the bregma; 1.5 mm depth). For each injection, 0.25 μl of BDA was delivered for a period of 30 s via a 15–20 μm inner diameter glass capillary attached to a microliter syringe (ITO Corporation). Two weeks after BDA injection, the animals were killed by perfusion with PBS followed by 4% paraformaldehyde. The spinal cords were dissected, postfixed overnight in the same fixa-

tives, and cryopreserved in 30% sucrose in PBS. A 20 mm length of spinal cord, 10 mm rostral and 10 mm caudal to the lesioned site, was embedded in Tissue-Tek OCT. These blocks were sectioned in the transverse plane (25 μm). Sections were incubated in PBS with 0.3% Triton X for 4 h and then incubated for 2 h with Alexa Fluor 488-conjugated streptavidin (1:400; Invitrogen) in PBS with 0.05% Tween 20. We then took serial cross sections of the spinal cord and quantitatively analyzed the distribution of the axons. Degrees of BDA uptake were assessed by counting the total number of fibers in the cross section 10 mm rostral to the lesioned site, where the CST was intact. For quantification of the number of labeled corticospinal axons 10 mm caudal to the lesion site, the number of labeled fibers was counted in the gray matter, the dorsal CST area (normal locations of the dorsal CST), or the white matter except for the dorsal CST area, and divided by the number of labeled corticospinal axons 10 mm above the lesion. The labeled fibers were counted using MetaMorph software (Molecular Devices Corporation). Light intensity and thresholding values were maintained at constant levels for all analyses.

Motor-evoked potential. In terminal electrophysiological experiments, after an intraperitoneal injection of ketamine (100 mg/kg), short trains of five square-wave stimuli of 0.5 ms duration at interstimulus intervals of 2 ms were delivered through the epidural electrode catheter at a point 10 mm rostral from the epicenter. The active electrode was placed in the muscle belly, and the reference electrode was placed near the distal tendon of the muscle in each gastrocnemius. The ground electrode was placed subcutaneously between the epidural electrode and the recording electrodes. The onset latency was measured as the length of time in milliseconds between the stimulus and the onset of the first wave. The duration was also measured as the length of time in milliseconds between the waves. One hundred responses were averaged and stored for off-line analysis.

Spinal cord-evoked potential after stimulation to the spinal cord. For sensory assessment, we performed spinal cord-evoked potential after stimulation to the spinal cord (sp-SCEP), which recognized extrapyramidal pathways including dorsal column axons (Sutter et al., 2007; Tamaki and Kubota, 2007). Stimulations were delivered through the epidural electrode catheter at a point 10 mm caudal from the epicenter and measured at a point 10 mm rostral from the epicenter. The ground electrode was placed subcutaneously between the epidural electrodes. The onset latency and peak latency were measured as the length of time in milliseconds between the stimulus and the onset and the peak of the first wave, respectively. A total of 100 responses were averaged and stored for off-line analysis of the latency.

Measurement of CS and KS. After freeze-drying, each specimen was digested with 0.7 ml of 2.5% actinase E (Kaken Pharmaceutical Corporation) at 55°C for 24 h. The digest was then kept at 100°C for 5 min and centrifuged at 3000 rpm for 10 min. The CS concentration was determined according to the description of Shinmei et al. (1992) with some modifications. A 0.2 ml aliquot of the supernatant was digested with 250 mU of C-ABC (Seikagaku) and 25 mU of chondroitinase AC-II (Seikagaku) in 20 mM Tris-HCl buffer, pH 8, at 37°C for 2 h. The sample was ultrafiltrated using a Nanosep centrifugal device (molecular size cutoff 10,000; PALL), and the filtrate, which contained the unsaturated disaccharides Δdi-0S, Δdi-4S, and Δdi-6S derived from CS, was analyzed by HPLC.

The KS concentration was measured according to the method of Shinmei et al. (1992) with some modifications. A 0.15 ml aliquot of the supernatant was digested with 1 mU of K-II (Seikagaku) in 20 mM sodium acetate buffer, pH 6, at 37°C for 3 h. The sample was then ultrafiltrated using a Nanosep centrifugal device, and the filtrate, which contained the saturated disaccharides β-galactosyl-(1–4)-6-*O*-sulfo-*N*-acetylglucosamine and β-6-*O*-sulfogalactosyl-(1–4)-6-*O*-sulfo-*N*-acetylglucosamine derived from KS, was analyzed by HPLC.

The HPLC system used in this study consisted of a Model 2000 high-performance chromatograph (Jasco) and a stainless steel column packed

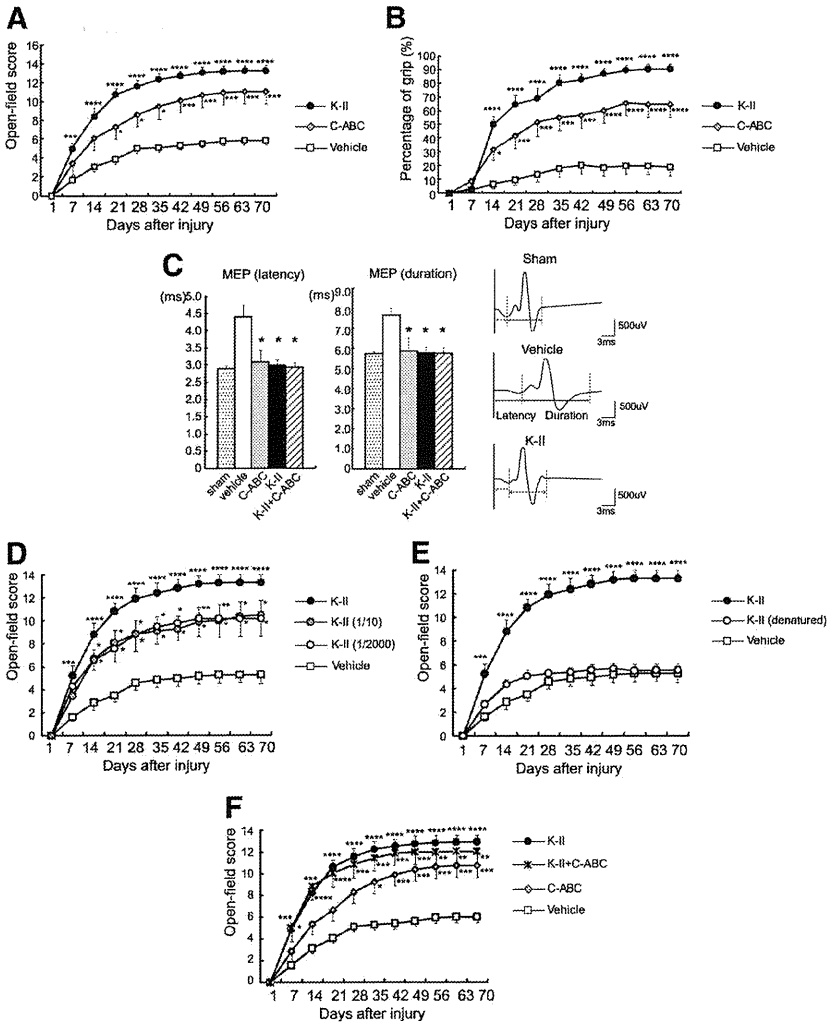

Figure 2. Motor function recovery by K-II after SCI. ***A***, ***B***, The BBB score and %grip test data after SCI. Recovery was significantly better in the K-II and C-ABC treatment groups than in the vehicle-administered control. Data represent the means ± SEM. $*p < 0.05$; $***p < 0.005$; $****p < 0.001$ versus the vehicle control ($n = 10$ K-II; $n = 7$ C-ABC; $n = 10$ Vehicle). ***C***, Electrophysiologic tests using MEP also showed functional recovery in the treatment groups at 8 weeks after SCI. Data represent the means ± SEM. $*p < 0.05$ versus the vehicle control ($n = 8$ Sham; $n = 9$ Vehicle; $n = 5$ C-ABC; $n = 7$ K-II; $n = 7$ K-II + C-ABC). ***D***, Motor function recovery after SCI in rats treated with K-II at various doses. K-II promoted functional recovery at a concentration of 0.05 U, and even restored motor function at concentrations of 0.005 U (1/10) and 0.0000025 U (1/2000). Data represent the means ± SEM. $*p < 0.05$; $**p < 0.01$; $***p < 0.005$; $****p < 0.001$ versus the vehicle control [$n = 7$ K-II; $n = 5$ K-II (1/10); $n = 6$ K-II (1/2000); $n = 7$ Vehicle]. ***E***, Heat-denatured K-II failed to promote motor function recovery after spinal cord injury. Data represent the means ± SEM. $***p < 0.005$; $****p < 0.001$ versus the vehicle control ($n = 7$ K-II; $n = 5$ Heat-denatured K-II; $n = 7$ Vehicle). ***F***, The combination of K-II and C-ABC did not show additive or synergistic effects on motor function (BBB score). Data represent the means ± SEM. $*p < 0.05$; $**p < 0.01$; $***p < 0.005$; $****p < 0.001$ versus the vehicle control ($n = 9$ Vehicle; $n = 7$ C-ABC; $n = 11$ K-II; $n = 7$ K-II + C-ABC).

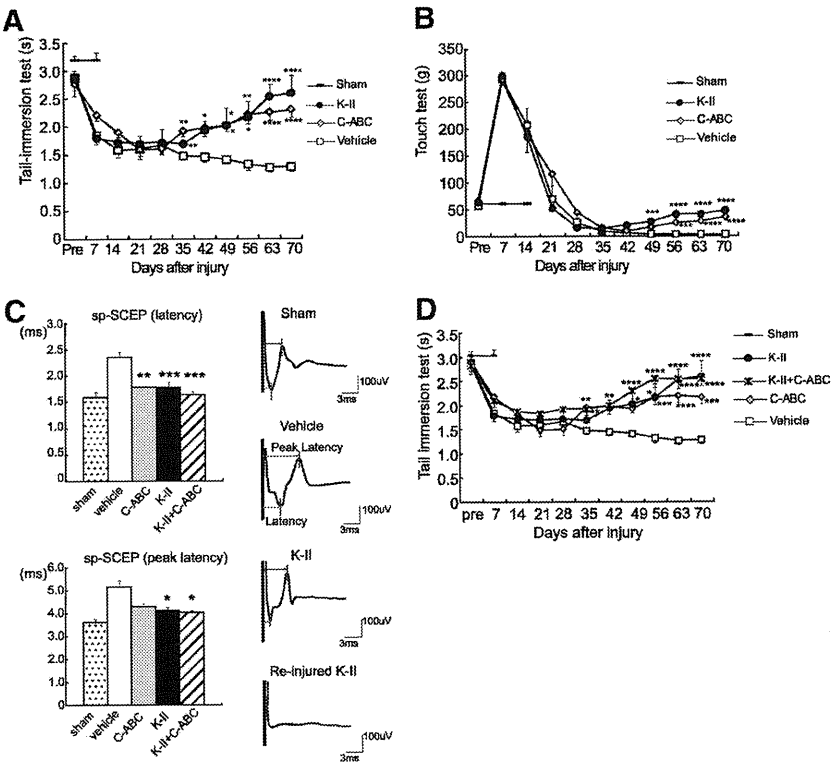

Figure 3. Sensory function recovery by K-II after SCI. ***A***, The tail-immersion test indicated that there was little allodynia in the K-II- and C-ABC-treated rats. Data represent the means ± SEM. $*p < 0.05$; $**p < 0.01$; $****p < 0.001$ versus the vehicle control ($n = 7$ Sham; $n = 5$ K-II; $n = 7$ C-ABC; $n = 9$ Vehicle). ***B***, The touch test also indicated that there was little allodynia in the K-II- and C-ABC-treated rats. Data represent the means ± SEM. $*p < 0.05$; $***p < 0.005$ versus the vehicle control ($n = 7$ Sham; $n = 5$ K-II; $n = 7$ C-ABC; $n = 9$ Vehicle). ***C***, Electrophysiologic tests using sp-SCEP showed not only motor functional recovery but also sensory recovery in the treatment groups at 8 weeks after SCI. The reinjury of K-II-treated rats lost the recovered response of sp-SCEP. Data represent the means ± SEM. $*p < 0.05$; $**p < 0.01$; $***p < 0.005$ versus the vehicle control ($n = 8$ Sham; $n = 7$ Vehicle; $n = 5$ C-ABC; $n = 6$ K-II; $n = 5$ K-II + C-ABC). ***D***, The combination of K-II and C-ABC did not show additive or synergistic effects on sensory function (tail-immersion test). Data represent the means ± SEM. $*p < 0.05$; $**p < 0.01$; $***p < 0.005$; $****p < 0.001$ versus the vehicle control ($n = 8$ Sham; $n = 9$ Vehicle; $n = 7$ C-ABC; $n = 11$ K-II; $n = 7$ K-II + C-ABC).

with polyamine-bound silica (YMC gel PA-120; YMC). The disaccharides in each sample were eluted with a gradient of 0–100 mM sodium sulfate. To the eluant from the column was added 100 mM sodium tetraborate buffer, pH 9, containing 1% 2-cyanoacetamide. The mixture was thermostated at 145°C, and the effluent was monitored by a fluoromonitor.

Cell culture. Sprague Dawley rats at postnatal days 7–9 were killed and their cerebella were collected. The meninges were carefully removed with fine forceps, and the tissues were minced and digested using a Papain Dissociation System (Worthington). Dissociated cells were applied to a 35/60% two-step Percoll gradient and centrifuged at 3000 × *g* for 15 min. Cerebellar granule neurons at the interface were collected. Cells were suspended in Neurobasal medium (Invitrogen) supplemented with 2% B27 (Invitrogen), 2 mM glutamine, an additional 20 mM KCl, 50 U/ml penicillin, and 50 μg/ml streptomycin.

Substrate preparation. Four-well chamber slides (Nunc) were coated with 20 μg/ml poly-L-lysine (PLL) (Sigma) and left overnight at 4°C. They were then coated with the indicated substrates and left for 4 h at 37°C. If indicated, proteoglycans or aggrecan were treated with 200 mU/ml C-ABC, 500 mU keratanase, and 5 mU/ml K-II derived from *Bacillus* sp. Ks36 or 5 mU endo-β-galactosidase (all from Seikagaku) in PBS at 37°C. Other substrate materials included poly-L-ornithine, aggrecan, and MAG (Sigma), Nogo and OMgp (R&D Systems), and KS and CS-C (Seikagaku).

Neurite outgrowth assay. Cerebellar granule neurons were seeded onto four-well chamber slides at 2.0×10^5/well. Twenty-four hours after seeding, the neurons were fixed with 4% paraformaldehyde/PBS and stained with anti-neuron-specific β-tubulin (Covance) to visualize the neurites. Neurite lengths were measured from at least 100 neurons per condition from duplicate wells, and quantified as described previously (Sivasankaran et al., 2004).

For reducing/alkylating proteoglycans, 5 μg of proteoglycans were suspended in 10 ml of 50 mM ammonium bicarbonate/PBS and reduced with 20 mM DTT for 60 min at 37°C. Then proteoglycans were alkylated with 10 mM iodoacetamide for 30 min at room temperature under dark condition. The proteoglycan solution was dialyzed against PBS for overnight and subjected to neurite outgrowth assay.

Preparation of GAG-BSA. CS-BSA was prepared as reported previously (Pumphrey et al., 2002) with minor modifications. Briefly, 20 mg of CS and 13 mg of BSA were linked using $NaBH_3CN$. CS-BSA was purified using anion-exchange chromatography (Q-Sepharose; GE Healthcare) followed by gel-filtration chromatography (Superose6 HR10/300; GE Healthcare) to remove free-BSA and free-CS, respectively. The protein concentration and KS concentration were quantified using a BCA Protein Assay Kit (Pierce) and HPLC analysis, respectively.

Because KS had an oligopeptide at its reducing end, we performed cross-linking between this peptide and BSA. Briefly, amino residues of this peptide were succinylated to inhibit self-cross-linking. Fifty-two milligrams of BSA and 20 mg of succinylated KS were cross-linked using *N*-hydroxysuccinimide (Pierce) and 1-ethyl-3-[3-dimethylaminopropyl]carbodiimide hydrochloride (Pierce). KS-BSA was purified using anion-exchange chromatography (Q-Sepharose; GE Healthcare) followed by gel-filtration chromatography (Superose6 HR10/300; GE Healthcare) to remove free-BSA and free-KS, respectively. The protein concentration and KS concentration were quantified using a BCA Protein Assay Kit (Pierce) and a Sulfated Glycosaminoglycan Quantification Kit (Seikagaku), respectively.

CS/KS-BSA was prepared by linking KS to CS-BSA.

Statistical analysis. We performed statistical analysis with an unpaired two-tailed Student's *t* test for single comparisons and one-way ANOVA for multiple comparisons. For the BBB score, %grip test, touch test, and tail-immersion test, we used repeated-measures ANOVA and Tukey's test. In all statistical analyses, significance was accepted at $p < 0.05$.

Results

In vitro and *in vivo* degradation of KS by K-II

We purified K-II from *B. circulans* as previously described (Yamagishi et al., 2003). Although the extracts of *B. circulans* showed both keratanase and chondroitinase activities, our stepwise protocol completely abolished the chondroitinase activity and purified K-II (Table 2). Furthermore, it is known that the purified enzyme does not digest hyaluronic acid, heparan sulfate, or heparin (Yamagishi et al., 2003). This enzyme is thermo-stable; indeed, it retained its enzymatic activity for at least 120 h at 37°C (100 ± 1.606% at 0 h vs 91.9 ± 4.014% at 120 h). Therefore, we decided to use this enzyme for *in vivo* experiments.

We asked whether K-II worked *in vivo*. To this end, we inflicted contusion injuries using a force of 200 kdyn in the rat spinal cord at the ninth thoracic vertebral level. This contusion model completely destroyed the dorsal columns and dorsal CST

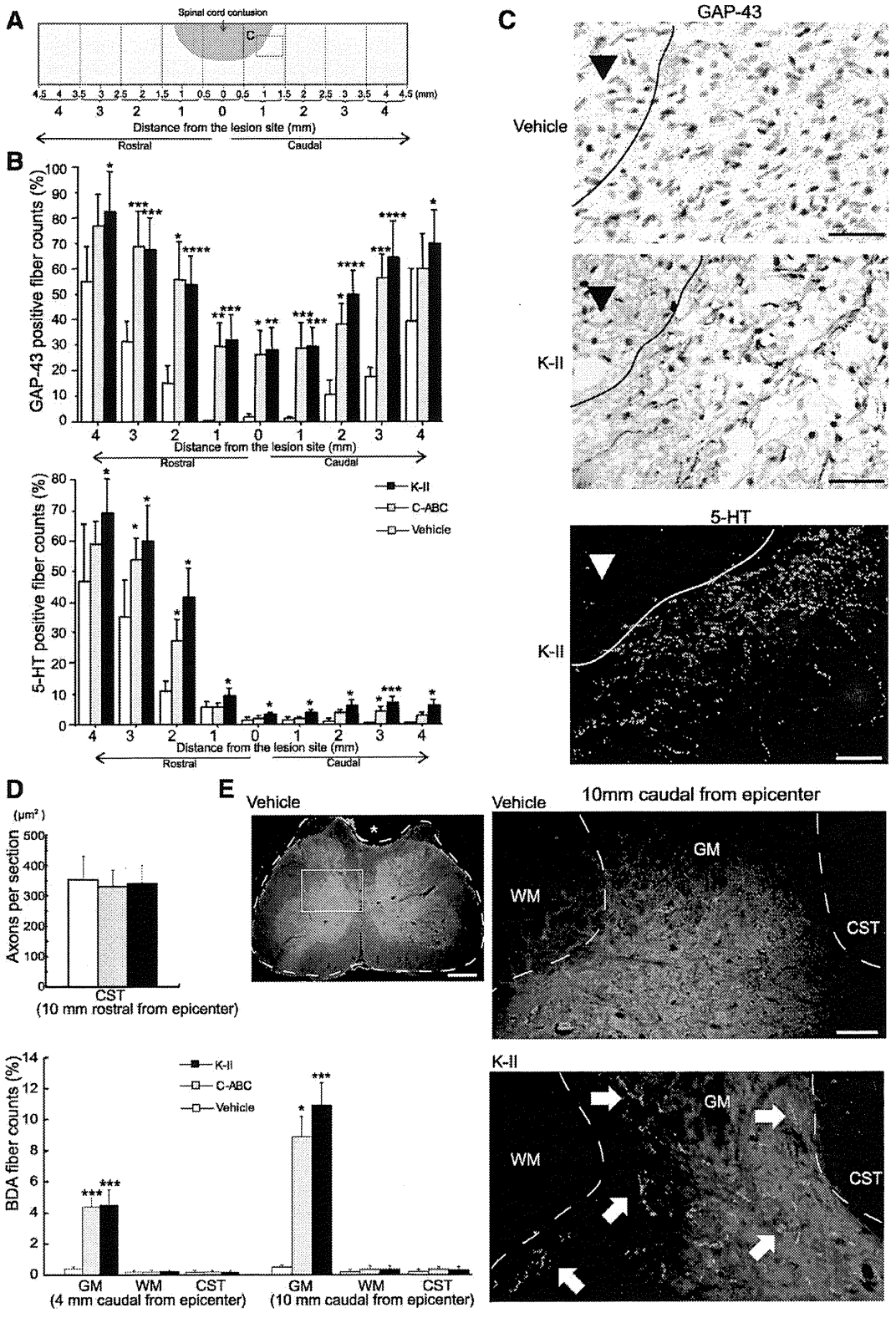

Figure 4. Histological analysis. ***A***, The scheme of the methods to reconstruct serial sagittal sections. On each section, the number of GAP-43- and 5-HT-positive fibers was counted from 4 mm rostral to 4 mm caudal the lesion site. The number was calculated as a percentage of the fibers seen in the sham-operated spinal cord. All serial sections were evaluated at 10 weeks after SCI. ***B***, Reconstruction of serial parasagittal section of the number of GAP-43- and 5-HT-positive fibers, represented as a percentage of the fibers seen in the sham-operated spinal cord. Data represent the means ± SEM. $*p < 0.05$; $**p < 0.01$; $***p < 0.005$; $****p < 0.001$ versus the vehicle control ($n = 5$ Vehicle; $n = 5$ C-ABC; $n = 6$ K-II). ***C***, Immunohistochemical analysis of GAP-43 and 5-HT (serotonin) expression in the injured spinal cord of the boxed area in scheme ***A*** at 10 weeks after SCI. Scale bars, 50 μm for the panels of GAP-43; 100 μm for the panel of 5-HT. All images are of sagittal section with the left side rostral. Arrowheads indicate the contusion area. ***D***, BDA labeling of CST. The top graph represents the number of labeled corticospinal (*Figure legend continues.*)